

Fullerenes | Very Important Paper |

VIP A Design Criteria to Achieve Giant Ising-Type Anisotropy in Co^{II}-Encapsulated MetallofullerenesMukesh Kumar Singh, Pratima Shukla, Munmun Khatua, and Gopalan Rajaraman*^[a]

Abstract: Discovery of permanent magnetisation in molecules just like in hard magnets decades ago led to the proposal of utilising these molecules for information storage devices and also as Q-bits in quantum computing. A significant breakthrough with a blocking temperature as high as 80 K has been recently reported for lanthanocene complexes. While enhancing the blocking temperature further remains one of the primary challenges, obtaining molecules that are suitable for the fabrication of the devices sets the bar very high in this area. Encouraged by the fact that our earlier predictions of potential single-molecule magnets (SMMs) in lanthanide-containing endohedral fullerenes have been verified, here we set out to undertake a comprehensive study on Co^{II}-ion-encapsulated fullerene as potential SMMs. To study this class of molecules, we have utilised an array of theoretical methods ranging from density functional to ab initio CASSCF/NEVPT2 methods for obtaining reliable estimate of zero-field splitting parameters *D* and *E*. Additionally, we have also employed, for the first time a combination of molecular


dynamics based on DFT methods coupled with CASSCF/NEVPT2 methods to seek the role of conformational isomers in the relaxation of magnetisation. Particularly, we have studied, Co@C₂₈, Co@C₃₈ and Co@C₄₈ cages and their isomers as potential target molecules that could yield substantial magnetic anisotropy. Our calculations categorically reveal a very large Ising anisotropy in this class of molecules, with Co@C₄₈ cages predicted to yield *D* values as high as -127 cm^{-1} . Our calculations on the smaller cages reveal the free movement of Co^{II} ion inside the cage, leading to the likely scenario of faster relaxation of magnetisation. However, larger fullerene cages were found to solve this issue. Further models with incorporating units such as {CoOZn}, {CoScZnN} inside larger fullerenes yield axial zero-field splitting values as high as -200 cm^{-1} with negligible *E/D* values. As these units represent a strong axiality coupled with a viable way to obtain air-stable low-coordinate Co^{II} complexes, this opens up a new paradigm in the search of SMMs in this class of molecules.

Introduction

Molecular magnets have attracted a great deal of attention in the last two decades as several potential applications to modernise current electronic devices have been proposed.^[1] Discovery of bi-stability for spin reversal of magnetisation in the first-ever reported single-molecule magnets^[2] at low temperatures led to the proposal of employing these molecules for molecular magneto-optical switches, extremely high-density and miniaturised information storage devices, quantum encryption devices, magnetic refrigeration, magnetic resonance imaging and recently in molecular spintronics.^[3] Only a handful of molecules based on transition metals are reported to possess a larger barrier height than the archetypal {Mn₁₂} cluster.^[2]

In transition-metal clusters, an SMM exhibiting a barrier height of 90 K has been reported, while for a two-coordinate Fe^{II} complex, the blocking barrier is found to be 4.5 K.^[4,5] In lanthanides, several Dy^{III} molecules possess substantial blocking temperature, and the value has now reached as large as 80 K.^[14,6] In this field, computational tools are indispensable as often calculations based on ab initio CASSCF based methods are utilised to rationalise the experimental properties.^[7] Moreover, these methods are robust towards prediction, and several such predictions made on lanthanide-encapsulated fullerene cages with varying size and shape has been duly verified by experimental groups.^[8] These lanthanide endohedral metallofullerenes (EMFs) are fullerenes that have metal ions, dinuclear fragments, trinuclear or mixed^[9] systems encapsulated in various C_n cages exhibiting fascinating magnetic properties.^[1k,8a,10] If doped fullerene cages such as C₇₉N are utilised, this leads to extremely strong magnetic coupling between the Ln^{III} and the radical centres, again predicted by theory and verified lately by experiments.^[1k,8b] Lanthanide ions are known to be anisotropic in nature because of the deeply buried degenerate 4f orbitals and by virtue of this property, they are found to be the most promising tool to build an SMM with high energy barrier for spin reversal.^[6d]

[a] Dr. M. K. Singh, P. Shukla, Dr. M. Khatua, Prof. G. Rajaraman
Department of Chemistry, Indian Institute of Technology Bombay
Powai, Mumbai 400076 (India)
E-mail: rajaraman@chem.iitb.ac.in

 Supporting information and the ORCID identification number(s) for the author(s) of this article can be found under:
<https://doi.org/10.1002/chem.201903618>. This contains optimised structure coordinates, AIM plots and tables, NEVPT2 + CASSCF computed energies, multi-determinant wave function of the ground and excited states for all studied cages and tables with anisotropy parameters.

Some transition-metal ions are also known to inherit large ground-state anisotropy reflected in the splitting of the metal states in zero-field along the particular direction and termed as axial zero-field splitting (D).^[1w,11] This anisotropy is strongly correlated to the coordination geometry around the metal ions and the electronic structure for the metal ions. Ligand-field-induced removal of d-orbital degeneracy causes lowering of axial anisotropy. Thus, obtaining a molecule with low coordination number can increase the anisotropy significantly by minimising the quenching of the orbital angular momentum by the ligand field. An illustrative example of this kind is the report of $[\text{Fe}^{\text{I}}\{\text{C}(\text{SiMe}_3)_3\}_2]^-$ and related compounds, reported to possess record high U_{eff} value for a transition-metal SMMs.^[5] Very recently, $[\text{Co}\{\text{C}(\text{SiMe}_2\text{ONaph})_3\}_2]$ has been reported in which a two-coordinate Co^{II} ion is found at the centre of the molecule, which possesses SMM characteristics with a reported U_{eff} value of 450 cm^{-1} .^[12] Though these examples illustrate clearly what can be achieved with transition-metal ions, all these complexes are unstable under ambient conditions and hence render future device fabrication using these molecules a herculean task.

An alternative and viable way to stabilise low-coordination transition-metal compounds is to encapsulate them in cages such as fullerene.^[8] Among the transition-metal complexes, Co^{II} complexes are found to be the most fascinating because of its strong ground state anisotropy, and several literature examples are already known for monometallic Co^{II} complexes with SMM properties with attractive barrier heights.^[13] Encapsulating the Co^{II} ion in EMFs thus is an attractive idea that can be pursued. In terms of natural abundance and relative ease of separation are further advantages in using cobalt as a substitute for lanthanide-based magnets. Considering that synthesis of the desired fragment inside the fullerene cage of apt size is a challenging task, screening such a large ensemble of molecules using ab initio CASSCF theory is an attractive idea to obtain lead molecules that are expected to possess interesting magnetic properties.

Moreover, literature precedent on transition/lanthanide single-ion magnets (SIMs) suggests the occurrence of several relaxation processes, such as quantum tunnelling of magnetisation (QTM), two-phonon Orbach and Raman relaxation, and relaxation due to metal/ligand nuclear spin (hyperfine coupling).^[6d] These cause the relaxation to occur with lower energy barrier leading to smaller blocking temperature (T_{B}), and is often much smaller than effective energy barrier, U_{eff} in SIMs. Among other factors that influence the QTM in transition-metal SIMs, transverse components of anisotropy (E) play an important role in controlling QTM.^[11b,14] Whereas, Orbach relaxation can be facilitated through higher excited states if one has strong axial ligand-field environment around metal ions in the absence or presence of very weak transverse ligand field. These stringent conditions to enhance the barrier height can be obtained using M@EMF as they have best of both worlds (strong axial direction, high-symmetry, no nuclear spin atoms such as H, which is very common in coordination complexes, high-rigidity due to strong carbon-carbon bond).^[8] For these reasons, here we have decided to employ the ab initio CASSCF

method to obtain insight into Co@EMFs and their suitability towards SMM behaviour. We aim to explore the following questions:

- 1) Which is the most suitable Co@EMF , among $\text{Co@C}_{28/38/48}$, to yield very large anisotropy?
- 2) Which is the most appropriate combination for F(C)-Co-X , here F(C) denotes fullerene C atoms and X oxygen or nitrogen atoms ($\text{CoNScZn@C}_{76/82}$ and $\text{CoOZn@C}_{70/80}$) among C_{70} , C_{76} , C_{80} and C_{82} that can be targeted to obtain large Ising anisotropy?
- 3) How stable are these cages and how does Co-C/O/N bonding influence the magnetic anisotropy?
- 4) As various isomers are possible for these Co@EMFs , how these geometric variations influence the magnetic anisotropy and eventually the QTM?
- 5) As the Co -cage bonds are often weak, the Co^{II} atom tends to move around the cage, creating various isomers. These isomers are correlated to the vibrational modes of the ground state structure. Among several cages studied, which structures fare better in obtaining consistently large negative zero-field splitting with a very small E/D values?

All these questions have been answered here using molecular dynamics based on DFT methods and combining these results with the calculations based on CASSCF/NEVPT2 methods on obtained geometries.

Results and Discussion

To begin with, we have started our computational studies on several endohedral Co^{II} fullerenes with varying cage size ranging from C_{28} to C_{82} and estimated their binding energies, structure and magnetic properties. We have performed calculations on all the selected EMFs and their isomers (see Figure 1). To ascertain how energetically close-lying isomers influence the magnetic anisotropy, we have considered all possible isomers of Co@C_{28} , Co@C_{38} and Co@C_{48} fullerenes in our calculations (there are two, six and nine isomers for these cages, respectively). All the estimated parameters are summarised in Table 1.

Structure and bonding in Co@C_{28} , Co@C_{38} and Co@C_{48} cages

C_{28} fullerene is known as one of the smallest stable fullerenes and literature examples are already known for metal encapsulated M@C_{28} types of molecules.^[6d,15] Two isomers are possible for C_{28} fullerene cage, and we have considered both of them ($\text{C}_{28}\text{-1}$ and $\text{C}_{28}\text{-2}$). We have placed a Co^{II} ion inside these isomers and performed geometry optimisation followed by single-point calculations to check the stability trend. $\text{Co@C}_{28}\text{-2}$ isomer is found to be more stable (by 32.9 kJ mol^{-1}) relative to $\text{Co@C}_{28}\text{-1}$. In isomer $\text{Co@C}_{28}\text{-1}$, the Co^{II} ion has highly distorted tetrahedral geometry. Whereas in the $\text{Co@C}_{28}\text{-2}$ isomer, the Co^{II} ion interacts with the η_6 hexagonal ring (see Figure 1). One can explain the observed stability trends using two key parameters: 1) strain in fullerene cage and 2) interaction between the endohedral Co^{II} ion with the carbon atoms of fullerene.

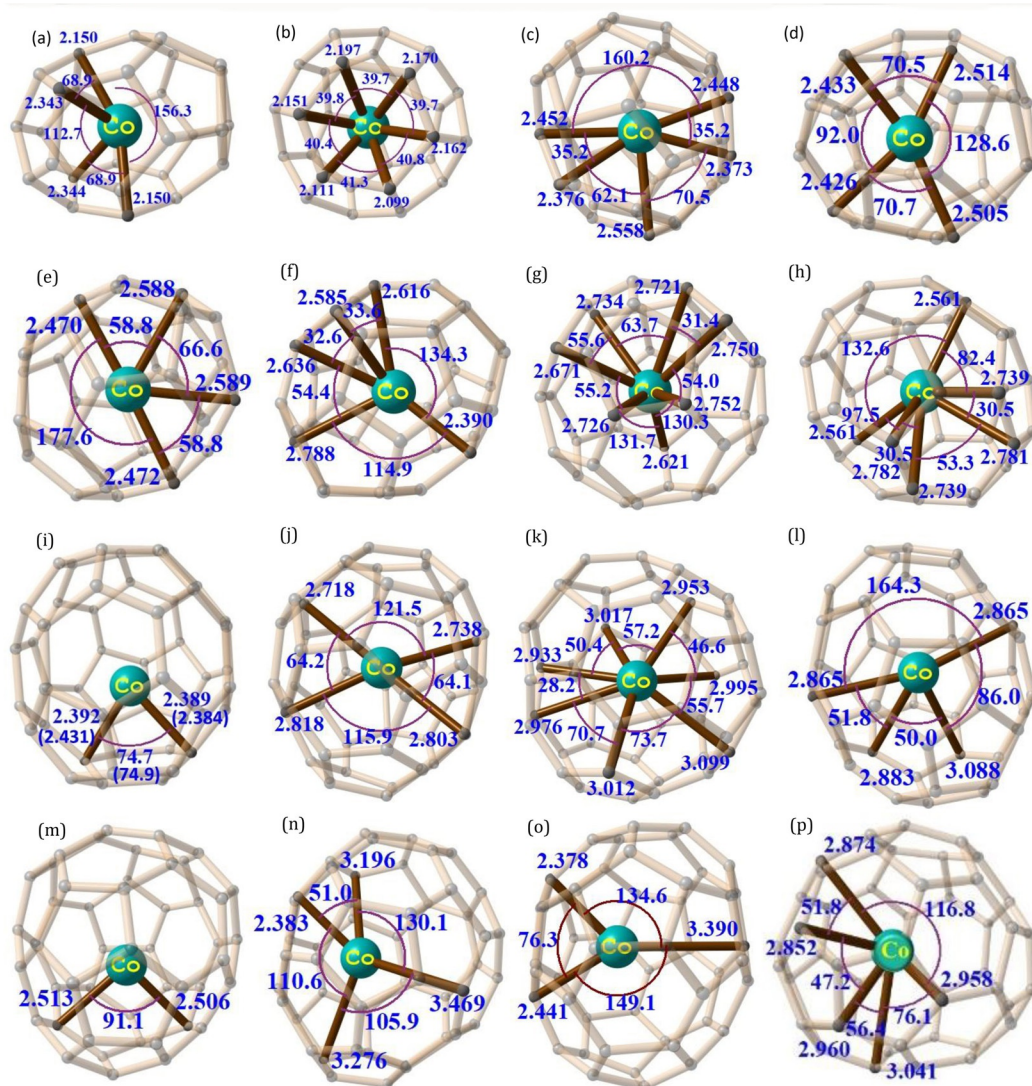


Figure 1. DFT optimised structures of a), b) Co@C₂₈-1, Co@ibC₂₈-2; c)–h) Co@C₃₈-1, Co@C₃₈-2, Co@C₃₈-3, Co@C₃₈-4, Co@C₃₈-5, Co@C₃₈-6; i)–p) Co@C₄₈-1-2, Co@C₄₈-3, Co@C₄₈-4, Co@C₄₈-5, Co@C₄₈-6, Co@C₄₈-7, Co@C₄₈-8 and Co@C₃₈-9 respectively with all the Co–C interactions obtained from AIM analysis and with all the important structural parameters. Colour code: Co^{II} cyan, O red and C dark grey.

The first parameter can be studied by considering the adjacent pentagonal ring count. Fullerenes with two pentagonal rings with one common fused adjacent are found to be destabilised because of the greater strain in the ring and this causes destabilisation by 75–150 kJ mol⁻¹ per adjacent pentagonal ring (APR or also known by isolated pentagonal rule, IPR).^[16] This factor is supposed to be the most influencing one as the magnitude of destabilisation is very large. The Co@C₂₈-1 isomer has 20 APR, whereas the Co@C₂₈-2 isomer has 18 APR, giving the extra stability for the latter isomer compared to the former one. The second parameter can be studied using natural bonding orbital (NBO) analysis. NBO donor–acceptor interactions in the second-order perturbation theory analysis yield four strong (Co)3d–(C)2p interactions (96.3 kJ mol⁻¹, 102.6 kJ mol⁻¹, 133.1 kJ mol⁻¹ and 147.0 kJ mol⁻¹) in the Co@C₂₈-2 isomer. These interactions are extremely small in Co@C₂₈-1 isomer suggesting additional electronic stabilisation in Co@C₂₈-2 due to the incorporation of Co^{II} ion (See Figure 2,

Table 1). Many other moderate interactions are present in both the isomers. Also, the Co@C₂₈-2 isomer has a smaller average Co–C distance compared to Co@C₂₈-1 isomer, suggesting the stronger Co–C interactions in the former isomer compared to the later isomer, as supported by NBO analysis.

Atom in molecules (AIM) analysis has been performed for both the isomers to get the insight into the bonding picture (see Figure S1 in the Supporting Information). AIM analysis suggests a comparatively strong Co–C(fullerene) covalent interactions for Co@C₂₈-2 relative to Co@C₂₈-1 (Figure 3 and Table 2). Figures S2 and S3 show the contour plots of electron density ($\rho(r)$) and Laplacian of the electron density ($\nabla^2\rho(r)$) of Co@C₂₈-1 and Co@C₂₈-2 molecules, respectively. Negative and positive values of $\nabla^2\rho(r)$ at the bond critical point (BCP) imply accumulation and depletion of electron density, respectively. Co@C₂₈-2 molecule has 6 BCPs, which are plotted along C₁₆–Co–C₁₈ (Figure 3 a & d), C₁₉–Co–C₂₂ (Figure 3 b & e) and C₂₇–Co–C₂₈ (Figure 3 c & f) planes.

Table 1. DFT calculated binding energies (kJ mol^{-1}) of all the studied fullerenes and EMFs along with their relative energies for the different isomers of the same molecules. (here, in $C_n\text{-M}$, n = number of carbon atoms in fullerene and M = isomer number) along with their NEVPT2 calculated D and E/D parameters. Second row gives the naming of the isomers as given in <http://www.nanotube.msu.edu/>. $\Delta E_{(\text{Co}+\text{EMF})-(\text{Co}@\text{EMF})}$ represents stabilisation energy or relief in the strain energy after encapsulation of Co^{II} ion.

Fullerene		$\Delta E_{\text{fullerene}}$	Co@EMF	$\Delta E_{\text{Co}@\text{EMF}}$	$\Delta E_{(\text{Co}+\text{EMF})-(\text{Co}@\text{EMF})}$	D [cm^{-1}]	E/D
$C_{28}\text{-1}$	$C_{28}\text{-D}_2\text{-1}$	5.2	Co@ $C_{28}\text{-1}$	32.9	2116.2	-24.3	0.28
$C_{28}\text{-2}$	$C_{28}\text{-T}_d\text{-2}$	0.0	Co@ $C_{28}\text{-2}$	0.0	2143.8	-72.4	0.00
$C_{38}\text{-1}$	$C_{38}\text{-C}_2\text{-6}$	205.6	Co@ $C_{38}\text{-1}$	192.3	2209.6	-50.7	0.20
$C_{38}\text{-2}$	$C_{38}\text{-C}_2\text{-10}$	0.0	Co@ $C_{38}\text{-2}$	12.6	2183.8	31.9	0.07
$C_{38}\text{-3}$	$C_{38}\text{-C}_2\text{-13}$	12.0	Co@ $C_{38}\text{-3}$	28.3	2180.1	-129.3	0.06
$C_{38}\text{-4}$	$C_{38}\text{-C}_1\text{-14}$	48.6	Co@ $C_{38}\text{-4}$	59.2	2185.7	-84.9	0.10
$C_{38}\text{-5}$	$C_{38}\text{-C}_3\text{-16}$	25.7	Co@ $C_{38}\text{-5}$	112.8	2109.3	-43.2	0.06
$C_{38}\text{-6}$	$C_{38}\text{-C}_2\text{-17}$	5.4	Co@ $C_{38}\text{-6}$	0.0	2201.7	-115.5	0.14
$C_{48}\text{-1}$	$C_{48}\text{-C}_2\text{-138}$	103.2	Co@ $C_{48}\text{-1}$	55.1	2143.0	-45.7	0.23
$C_{48}\text{-2}$	$C_{48}\text{-C}_1\text{-139}$	127.7	Co@ $C_{48}\text{-2}$	56.9	2165.7	41.1	0.21
$C_{48}\text{-3}$	$C_{48}\text{-D}_2\text{-169}$	169.6	Co@ $C_{48}\text{-3}$	96.0	2168.5	-104.7	0.02
$C_{48}\text{-4}$	$C_{48}\text{-C}_2\text{-170}$	25.8	Co@ $C_{48}\text{-4}$	6.4	2114.2	-57.5	0.18
$C_{48}\text{-5}$	$C_{48}\text{-C}_2\text{-171}$	54.5	Co@ $C_{48}\text{-5}$	12.3	2137.1	-115.0	0.04
$C_{48}\text{-6}$	$C_{48}\text{-C}_2\text{-194}$	188.6	Co@ $C_{48}\text{-6}$	116.6	2166.8	58.4	0.25
$C_{48}\text{-7}$	$C_{48}\text{-C}_1\text{-195}$	133.3	Co@ $C_{48}\text{-7}$	85.6	2142.6	-69.9	0.06
$C_{48}\text{-8}$	$C_{48}\text{-C}_5\text{-197}$	108.2	Co@ $C_{48}\text{-8}$	39.5	2163.7	-78.3	0.05
$C_{48}\text{-9}$	$C_{48}\text{-C}_2\text{-199}$	0.0	Co@ $C_{48}\text{-9}$	0.0	2094.9	-69.9	0.04

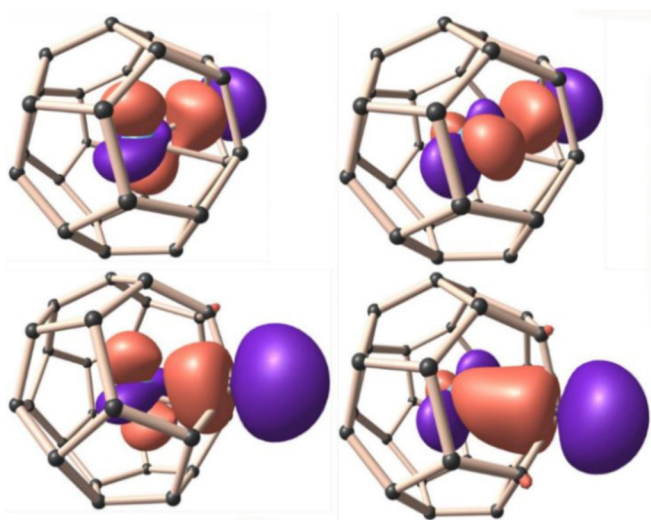


Figure 2. Four strong donor–acceptor interactions computed for $(\text{Co})3d\text{--}(C)2p$ interactions in $\text{Co}@\text{C}_{28}\text{-2}$.

We have considered six isomers for the $\text{Co}@\text{C}_{38}$ fullerene. The most stable isomer, $\text{Co}@\text{C}_{38}\text{-6}$, in which Co^{II} ion is found to be in highly distorted six coordinated reverse umbrella geometry, is followed by the $\text{Co}@\text{C}_{38}\text{-2}$ isomer (by a margin of 12.6 kJ mol^{-1}) in which the Co^{II} ion is in distorted square planar geometry (see Figure 1 for the geometry around Co^{II} ion in other isomers). All other isomers have a relative energy of more than 28 kJ mol^{-1} with respect to the lowest energy structure (Table 1). Isomer $\text{Co}@\text{C}_{38}\text{-6}$ has 11 APRs whereas isomers $\text{Co}@\text{C}_{38}\text{-2}$, $\text{Co}@\text{C}_{38}\text{-3}$, $\text{Co}@\text{C}_{38}\text{-4}$ and $\text{Co}@\text{C}_{38}\text{-5}$ have 12 APRs. $\text{Co}@\text{C}_{38}\text{-1}$ isomer has 14 APR numbers. This and the nature of $\text{Co}\text{--C}$ bonding interactions as deduced from NBO ($2372.7 \text{ kJ mol}^{-1}$ vs. $2185.5 \text{ kJ mol}^{-1}$ for $\text{Co}\text{--C}$ bond in $\text{Co}@\text{C}_{38}\text{-6}$ isomer vs. $\text{Co}@\text{C}_{38}\text{-1}$) explain the energetics trend obtained

from the calculations. AIM analysis reveals six BCPs for $\text{Co}@\text{C}_{38}\text{-6}$ (see Figures S1 and S3 and Table S1 of the Supporting Information for the contour diagram and values) and this clearly reveals that as the cage size increases from C_{28} to C_{38} , the strength of the $\text{Co}\text{--C}$ interactions diminish.

We have considered nine isomers for $\text{Co}@\text{C}_{48}$ fullerene and here $\text{Co}@\text{C}_{48}\text{-9}$ isomer is found to be the most stable, with Co^{II} ion in highly distorted square pyramidal geometry, followed by the isomers $\text{Co}@\text{C}_{48}\text{-4}$ and $\text{Co}@\text{C}_{48}\text{-5}$, which are 6.4 and 12.3 kJ mol^{-1} higher in energy, respectively with Co^{II} ion in seven coordinated distorted capped trigonal anti-prism and four coordinated distorted T-shape geometries, respectively (see Table 1, see Figure 1 for the geometry around Co^{II} ion in other isomers). All other isomers are found to be high-lying (more than ca. 40 kJ mol^{-1}). As stated earlier, the stability trend can be explained using structural topology, NBO donor–acceptor interactions and AIM analysis. Here AIM analysis reveals that the most stable $\text{Co}@\text{C}_{48}\text{-9}$ has six BCPs (see Figures S1 and S4 and Table S2 of Supporting Information for the contour diagram and values); however, the strength of such interactions is weaker compared to C_{28} and C_{38} cages. Incorporation of Co^{II} ion tends to stabilise an isomer which is otherwise slightly high-lying in energy in case of C_{38} isomers; however, this is not true for C_{28} and C_{48} cages. While the incorporation of Co^{II} and formation of a $\text{Co}^{\text{II}}\text{--carbon}$ bond was found to ease some of the strain (see Table 1), it is very clear from comparing the trend that the energetically high-lying cages with a large energy margin with respect to the ground state geometry are unlikely to be stabilised by the metal encapsulation.

Estimation of zero-field splitting in $\text{Co}@\text{C}_{28}$, $\text{Co}@\text{C}_{38}$ and $\text{Co}@\text{C}_{48}$ cages

While large magnetic anisotropy for Co^{II} ion in various coordination numbers has been reported,^[11a,d,e,12,17] how the anisotropy

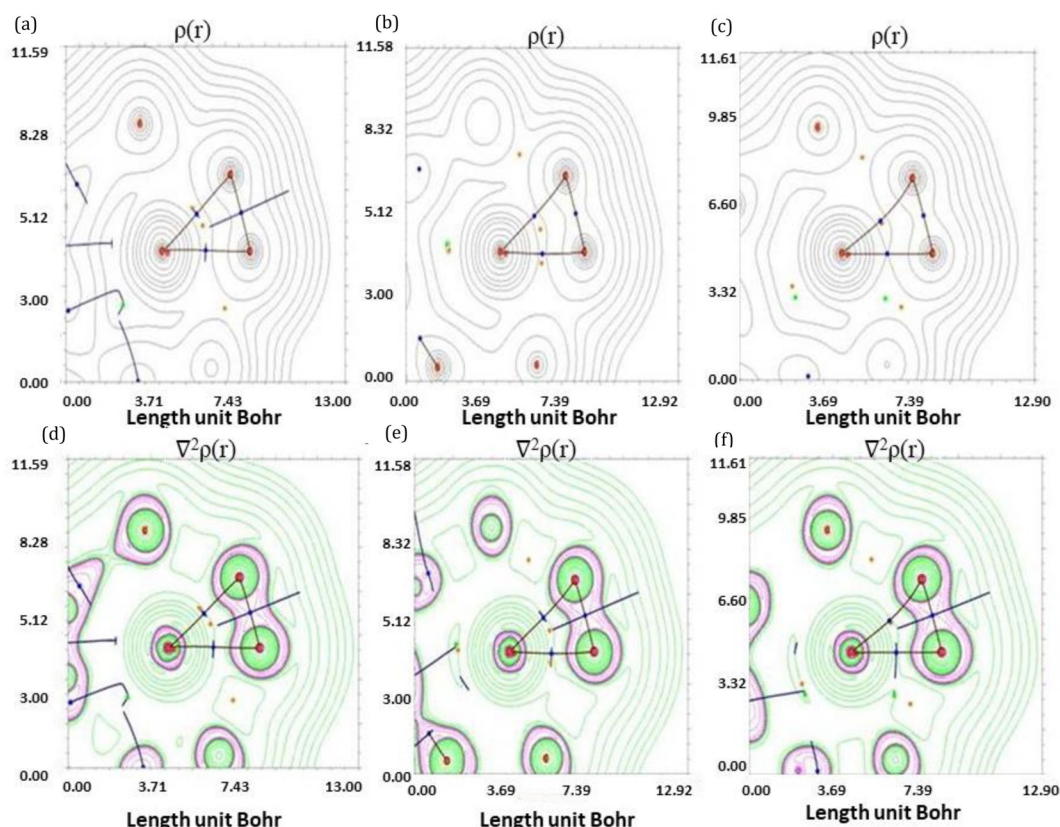


Figure 3. Plots of electron density $\rho(r)$ and Laplacian of electron density ($\nabla^2\rho(r)$) for Co@C₂₈-2 a), d) with BCPs between Co–C16 and Co–C18, b), e) with BCPs between Co–C19 and Co–C22 and c), f) with BCPs between Co–C27 and Co–C28. The black lines in (a, b and c) indicate $\rho(r)$, green and magenta lines in d), e) and f) indicate $\nabla^2\rho(r) > 0$ and $\nabla^2\rho(r) < 0$ region, respectively. Blue dots indicate BCPs, brown lines indicate MEP (maximum electron density path) between Co–C and blue lines indicate inter basin paths.

Table 2. Bond critical point (BCP) properties in Co@C₂₈-1 and Co@C₂₈-2 molecules.

	Co–C	$\rho(r)^{[a]}$ [ea ₀ ⁻³]	$\nabla^2\rho(r)^{[b]}$ [ea ₀ ⁻⁵]	$G(r)^{[c]}$ [ea ₀ ⁻¹]	$H(r)^{[d]}$ [ea ₀ ⁻⁴]
Co@C ₂₈ -1	Co–C6	0.0685	0.2186	0.074	–0.0194
	Co–C12	0.048	0.1727	0.0515	–0.0083
	Co–C16	0.0685	0.2187	0.074	–0.0193
	Co–C26	0.0479	0.1725	0.0514	–0.0083
Co@C ₂₈ -2	Co–C16	0.0643	0.22408	0.0713	–0.0153
	Co–C18	0.0685	0.21505	0.0724	–0.0187
	Co–C19	0.072	0.22404	0.0762	–0.0202
	Co–C22	0.0749	0.25771	0.0866	–0.0222
	Co–C27	0.0796	0.2402	0.086	–0.0259
	Co–C28	0.0697	0.2304	0.0757	–0.0181

py can be modulated in a cage structure such as in EMF has not been reported. These metal encapsulating fullerenes are expected to maintain a low coordination environment around the metal ion ensuring stability at ambient conditions—an extremely rare combination and hard to achieve in classical coordination compounds. Literature examples show the presence of both easy axis (negative D) and easy plane (positive D) systems for monometallic Co^{II} complexes depending on geometry and ligand field effects.^[11d]

For Co@C₂₈ cages, the dominant ground state electronic arrangement for isomers Co@C₂₈-1 and Co@C₂₈-2 are $(d_{yz})^2(d_{xy})^2(d_{x^2-y^2})^1(d_{z^2})^1(d_{zz})^1$ and $(d_{z^2})^2(d_{x^2-y^2})^2(d_{xy})^1(d_{xz})^1(d_{yz})^1$ with 60% and 56% contributions, respectively. The ground state wavefunction for Co^{II} complexes are composed of several determinants and some of these determinants are non-Aufbau in nature^[12] and here as well the ground state electronic configuration is found to be strongly mixed with $(d_{yz})^2(d_{xy})^2(d_{x^2-y^2})^1(d_{z^2})^1(d_{zz})^1$ and $(d_{z^2})^2(d_{x^2-y^2})^2(d_{xy})^1(d_{xz})^1(d_{yz})^1$ configurations (12% and 14% mixing, respectively for Co@C₂₈-1 and Co@C₂₈-2) to the ground state wavefunction (see Figure 4 and Table S3 for all other possible electronic arrangements and their contributions). Similar to the ground state, the first excited state which contributes most to the D parameters also found to have strong multi-determinantal characteristics (see Figure 4 and Table S3). The calculated D values for both the isomers are found to be negative and the Co@C₂₈-2 isomer has a D value almost three times larger than the Co@C₂₈-1 isomer (72.4 cm⁻¹ and 24.3 cm⁻¹, respectively). This drastic variation in D observed between these two isomers can be related to the nature of Co–C bonding with Co@C₂₈-1 exhibiting heavily distorted square-planar geometry, while Co@C₂₈-2 has an η_6 coordination with a hexagonal ring. This geometric difference in Co@C₂₈-2 destabilises the $d_{x^2-y^2}$ orbital and stabilises the d_{xy} orbital compared to Co@C₂₈-1. For both isomers, the largest con-

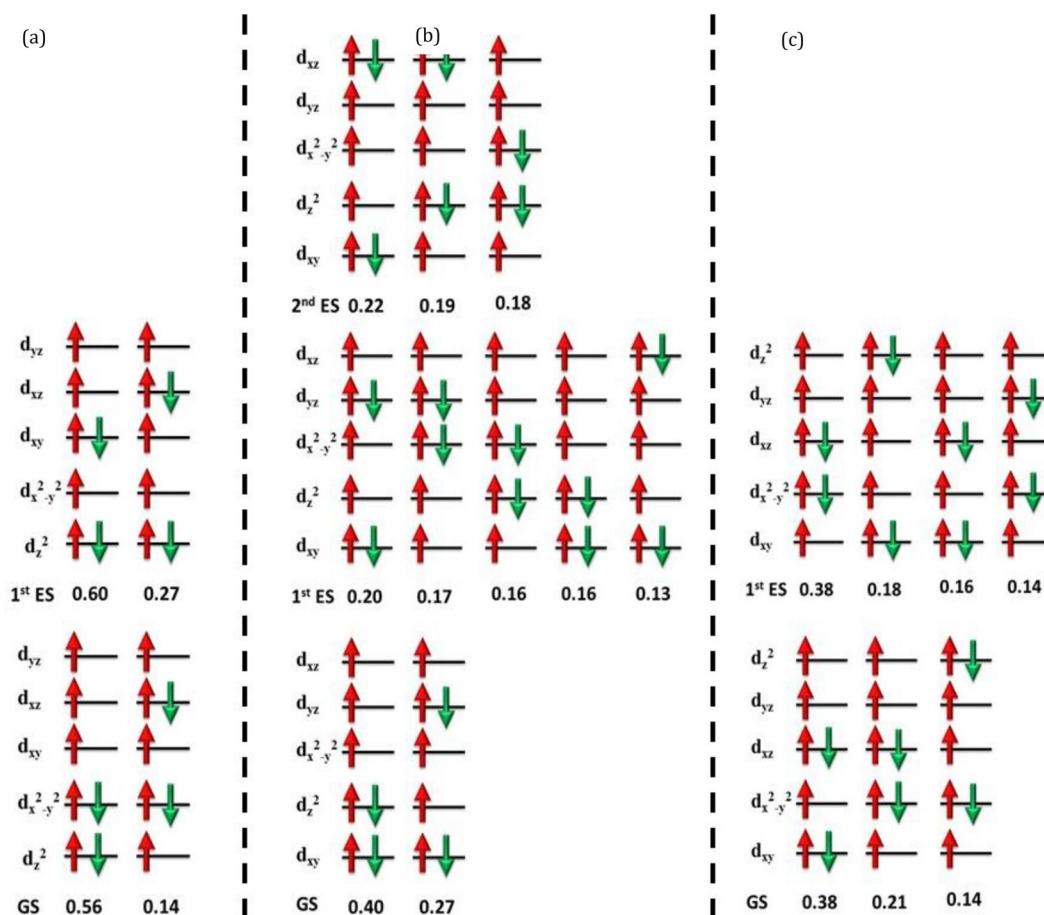


Figure 4. Multi-determinant characteristics of the ground and excited state wave function for a) Co@C₂₈-2, b) Co@C₃₈-6 and c) Co@C₄₈-9. The computed CI coefficients that are larger than 10% are shown above. For other molecules the results are summarised in a tabular form given in Supporting Information (see Table S3).

tribution arises from $d_{x^2-y^2} \rightarrow d_{xy}$ transition, as these orbitals are very close-lying in energy and the negative sign of D can also be rationalised as this transition is between same m_l levels.^[18] In Co@C₂₈-1, energy separation between these two orbitals is found to be larger (3404 cm⁻¹ vs. 526.7 cm⁻¹ for Co@C₂₈-1 and Co@C₂₈-2 isomers, respectively, see Figure 5a and Table S4–5) compared to Co@C₂₈-2 isomer resulting in large negative D value for the latter.

Another important point to mention here is the trend in the magnitude and sign of D observed for CASSCF and NEVPT2 are found to be similar for both isomers.^[19] The E/D value for Co@C₂₈-1 isomer is found to be relatively large (0.23) and this is likely to lead to a faster relaxation of magnetisation. In Co@C₂₈-2 isomer, the E/D value is estimated to be close to zero. Because of the large negative D along with zero E/D value, the Co@C₂₈-2 isomer is an ideal target within this small cage for superior SMM characteristics (negligible E/D , no atom that contains nuclear spin to offer hyperfine interaction to facilitate the QTM except Co and capsulation likely to also diminish the possible intermolecular interactions). This change of E parameter is explained later.

NEVPT2 calculations on Co@C₃₈ cages suggest isomers Co@C₃₈-1, Co@C₃₈-3, Co@C₃₈-4, Co@C₃₈-5 and Co@C₃₈-6 possess

negative D values. For isomer Co@C₃₈-2, the D value is found to be positive. The dominant ground state electronic arrangement for isomers Co@C₃₈-1, Co@C₃₈-3, Co@C₃₈-4, Co@C₃₈-5 and Co@C₃₈-6 is found to be $(d_{xy})^2(d_{yz})^2(d_{x^2-y^2})^1(d_{xz})^1(d_z^2)^1$, $(d_{x^2-y^2})^1(d_{yz})^2(d_{xy})^2(d_z^2)^1(d_{xz})^1$, $(d_{xy})^2(d_{x^2-y^2})^1(d_z^2)^2(d_{yz})^1(d_{xz})^1$, $(d_{x^2-y^2})^1(d_{yz})^1(d_{xy})^2(d_{xz})^2(d_z^2)^1$ and $(d_{xy})^2(d_z^2)^2(d_{x^2-y^2})^1(d_{yz})^1(d_{xz})^1$ with 95%, 41%, 66%, 29% and 40% contributions, respectively. In these isomers, the largest contribution to D comes from $d_{xy}/x^2-y^2 \rightarrow d_{x^2-y^2}/xy$ and $d_{yz}/yz \rightarrow d_{yz}/xz$ transitions. The magnitude of D can be explained based on the energy separation between orbitals among which electron transition occurs. Smaller the energy separation between these orbitals, larger will be the magnitude of D and vice versa (see Figure 5b). For Co@C₃₈-2 isomer, the dominant ground state electronic arrangement is calculated to be $(d_z^2)^1(d_{x^2-y^2})^2(d_{xy})^2(d_{xz})^1(d_{yz})^1$ with 36% contribution. The electronic transition from $d_{x^2-y^2} \rightarrow d_{xz}$ is prominent and yield positive contribution to D . Except for isomers Co@C₃₈-1 and Co@C₃₈-4, in all other isomers, ground (except Co@C₃₈-1) and first excited states are strongly mixed suggesting unquenched orbital contribution leading to larger D values (see Figure 4 and Table S3). In isomers Co@C₃₈-1 and Co@C₃₈-4, the major contribution to the D parameter comes from a regular Aufbau determinant. Due to the larger size of the cage in

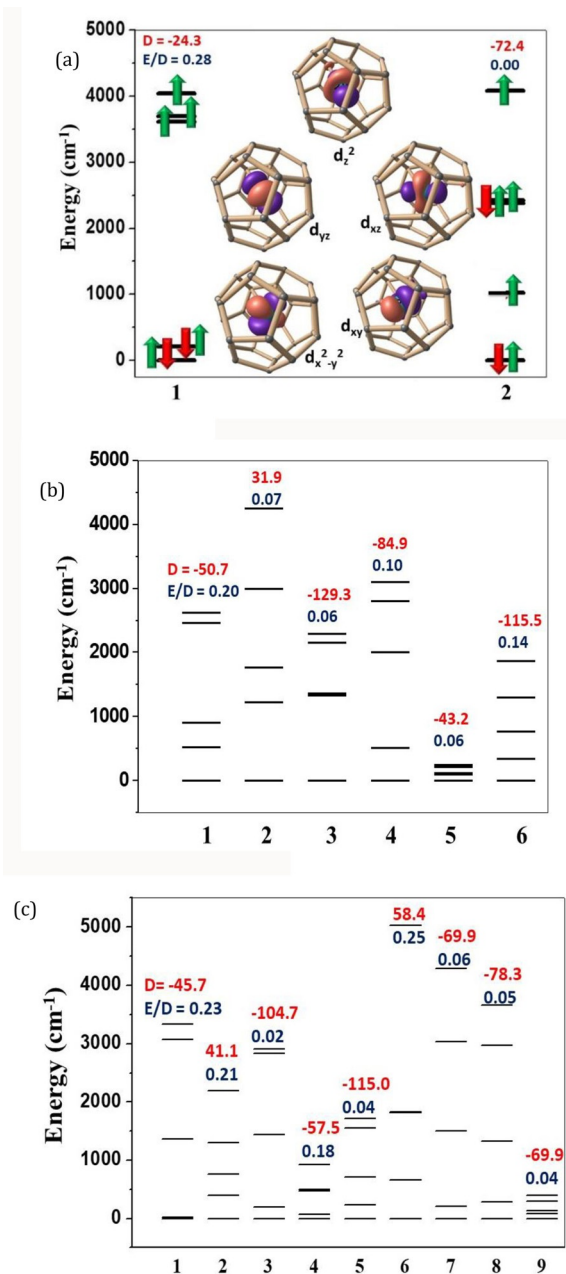


Figure 5. a)–c) Computed d-orbitals splitting for all studied isomers of Co@C₂₈, Co@C₃₈ and Co@C₄₈ respectively. The values written above the diagrams are computed D (red) and E/D (dark blue) values. Note here that for both isomers only the predominant ground state configuration is represented.

Co@C₃₈, one can expect a weakening of both transverse and axial Co–C ligand field strength. However, Co–C interactions in the transverse direction are found to be weaker than the axial, as revealed by the AIM analysis. This results in the overall increase in the magnitude of D for Co@C₃₈ compared to Co@C₂₈ fullerene.

For Co@C₄₈ cages, NEVPT2 calculations suggest isomers Co@C₄₈-2 and Co@C₄₈-6 have positive D values. For the remaining seven isomers, the D value is found to be negative. The dominant ground state electronic arrangement for isomers Co@C₄₈-1, Co@C₄₈-3–5, Co@C₃₈-7–9 is found to be

$(d_{x^2-y^2})^2(d_{xz})^2(d_{xy})^1(d_{z^2})^1(d_{yz})^1$, $(d_{x^2-y^2})^2(d_{xy})^1(d_{z^2})^2(d_{yz})^1$, $(d_{x^2-y^2})^1(d_{xy})^2(d_{xz})^1(d_{z^2})^2(d_{yz})^1$, $(d_{xy})^2(d_{x^2-y^2})^1(d_{z^2})^2(d_{xz})^1(d_{yz})^1$, $(d_{xy})^2(d_{x^2-y^2})^1(d_{z^2})^2(d_{z^2})^1$ and $(d_{xy})^2(d_{x^2-y^2})^1(d_{xz})^2(d_{yz})^1(d_{z^2})^1$ with 61%, 100%, 34%, 75%, 57%, 91% and 38% contributions, respectively. Like most of the Co@C₃₈ isomers, the largest contribution to D comes from $d_{xy/x^2-y^2} \rightarrow d_{x^2-y^2/xy}$ and $d_{xz/yz} \rightarrow d_{yz/xz}$ transitions. The magnitude of D can be explained based on the energy separation between the orbitals among which electron transition takes place (see Figure 5 c). For Co@C₄₈-2 and Co@C₄₈-6, the dominant ground state electronic arrangement is calculated to be $(d_{xy})^2(d_{x^2-y^2})^1(d_{z^2})^1(d_{yz})^2(d_{z^2})^1$ with 35% and 80% contributions, respectively. Electronic transition from $d_{xy} \rightarrow d_{xz}$ is prominent in these two structures, yielding positive contribution to D . In all these isomers, ground (except Co@C₄₈-3, Co@C₄₈-5, Co@C₄₈-6 and Co@C₄₈-8) and first excited (except Co@C₄₈-3, Co@C₄₈-6 and Co@C₄₈-8) states are strongly mixed yielding large D values (see Figure 4 and Table S3). Compared to Co@C₃₈ and Co@C₂₈ cages, the Co@C₄₈ cage size is larger, leading to a weaker Co–C ligand field interaction (from AIM analysis), resulting in the overall/average decrease in the magnitude of D for Co@C₄₈. It is important to note here that in all these Co^{II} ion encapsulated cages, the large D parameter is attributed to either the regular Aufbau determinant (with small energy separation between 3d-orbitals which are involved in electronic transition) along with multideterminantal non-Aufbau ground-excited states together or individually (see Figures 4 and 5 and Tables S3–S20).

The E values are generally found to be negative and independent of the size of the cage. The most dominant contribution comes from transitions between orbitals that have different m_l values ($d_{x^2-y^2/xy} \rightarrow d_{xz/yz}$ transitions). The positive contribution to the E parameter is found to arise when the transition involves two orbitals of the same m_l values ($d_{x^2-y^2/xy} \rightarrow d_{xy/x^2-y^2}$ or $d_{xz/yz} \rightarrow d_{yz/xz}$ transitions). One should expect very small E parameter if both the contributions are comparable as in Co@C₂₈-2 isomer (see Figure 5 a, Table S3 and S5). Compared to spin conserved transitions, spin-flip contributions to both D and E parameters are found to be smaller because of large energy separation between the quartets and doublets states (see Figure S5 and Table S4–20 of the Supporting Information).

Ab initio molecular dynamic (MD) simulation of Co@C₂₈, Co@C₃₈ and Co@C₄₈ cages

Several models considered here yield very large negative D and very small E/D values as desired for SMMs. However, very often relaxation mechanism for such cases are non-Orbach in nature leading to relaxation through vibrationally excited states. This has been illustrated in a four-coordinate Co^{II} complex reported earlier.^[13c]

In EMFs such as the one studied here apart from other effects, there are several possible isomers that can interconvert from one to other isomers with very small energy barrier and the Co^{II} ion inside the cage can move to result in various states with lower D and large E/D values. To ascertain the factors that could facilitate such relaxation, we decided to per-

form ab initio molecular dynamics simulation using density functional methods (using UB3LYP functional). We performed molecular dynamics simulations on the lowest energy structure of $\text{Co}@C_{28/38/48}$ cages ($\text{Co}@C_{28}\text{-2}$, $\text{Co}@C_{38}\text{-6}$ and $\text{Co}@C_{48}\text{-9}$) for 500 to 1000 fs at 300 K temperature. From the simulated data, we carefully looked at the MD trajectories and selected various geometries that lie closer in energy to the ground state structure for the calculation of D and E/D parameters. In this approach, we aim to see the robustness of the cage size and how various dynamical configurations could offer shorter relaxation pathways compared to the ground state structures.

The MD trajectory obtained for $\text{Co}@C_{28}\text{-2}$ isomer is shown in Figure 6a, in which energy difference with respect to the lowest energy isomer is plotted against time. The dynamics clearly reveal that Co^{II} ion moves within the cage rather easily—it started moving towards the wall of the cage and then retracted back towards the centre resulting in maximum and minimum points in the energy plot, respectively. As it comes closer to the wall of the cage, the energy rises due to

repulsion between the C atoms of the cage and the Co^{II} ion and falls when it moves away (see Figure 6b). Due to this, oscillations are observed in the energy plot. The cage distorts when the Co^{II} ion approaches the wall of the cage which also attributes to the oscillations in the energy plot. There is a maximum at 12 fs, which may be due to the fact that the minimum energy molecular system takes 12 fs of time to move out of the potential well. Table S21 in Supporting Information shows the diameters of the cage, the shortest and the longest Co–C distances at different time steps. From the table, we see that at the start of the simulation up to 130 fs, the movement of the Co^{II} ion inside the cage is more prominent than the later stages of the simulation. At 46, 50 and 58 fs, the Co^{II} ion is closest to the wall of the cage than at other time steps. This is well reflected in the energy plot where the energy reaches a maximum point at 58 fs. The distortion in the cage can be measured by the difference in the diameter of the cage. The distortions of the cage at 46, 50 and 58 fs are more than the rest of the geometry. This may be the reason behind the irregular variation in energy up to 130 fs. After 130 fs, the energy oscillates within a fixed range. Within the initial 8 fs, the geometry around Co^{II} ion is found to be $\eta_{6/5}$ coordination with a hexagonal ring, which is very close to the geometry of $\text{Co}@C_{28}\text{-2}$ isomer. In the next time scales, the Co^{II} ion is found to move closer towards the adjacent pentagonal ring leading to various geometries. (see Figure S8 in the Supporting Information for various geometries).

Figure 6c provides the time evolution of total energy for the stable isomer $\text{Co}@C_{38}\text{-6}$ after performing an AIMD simulation at 300 K and a similar oscillation also observed for this isomer (see Figure 6d). Here also in the initial 6 fs, the geometry around Co^{II} ion is found to be same as isomer $\text{Co}@C_{38}\text{-6}$ with a small decrease in the Co–C bond length with time, resulting in a slight increase in the magnetic anisotropy (see Figure S8 in the Supporting Information). The data collected for $\text{Co}@C_{48}\text{-9}$ is shown in Figure 6e. Unlike the other two cages, here oscillations are seen, but at a larger time scales, reflecting greater stability of the Co^{II} ions in a particular geometry. Larger cage size aid movement of Co^{II} ion albeit slowly and generates fewer numbers of minima compared to the other two cages and this has a significant impact on the mechanism of relaxation (see Figure 6f). To assess the magnetic anisotropy of various snapshots obtained from MD, we have analysed the data and taken into consideration those structures which are energetically close lying to the ground state structure (within an energy window of 80 kJ mol^{-1} or $\approx 6690 \text{ cm}^{-1}$) and computed D and E/D . For $\text{Co}@C_{28}\text{-2}$ molecule, MD reveals that there are eighteen geometries occurring at various time scales. Particularly in the window of 1–8 fs time scale, eight geometries are found while in 29–30; 97–98; 130–131 fs time scale two geometries are found. In 78–80 fs scale, three geometries are found. Our geometry analysis and also the calculations of D and E/D on these snapshots reveal that within the given time scale window, the isomers have only minor structural perturbations and hence the parameters computed are very similar. Hence we will analyse only one point each for the anisotropy. For isomers $\text{Co}@C_{38}\text{-6}$ and $\text{Co}@C_{48}\text{-9}$, only five and two struc-

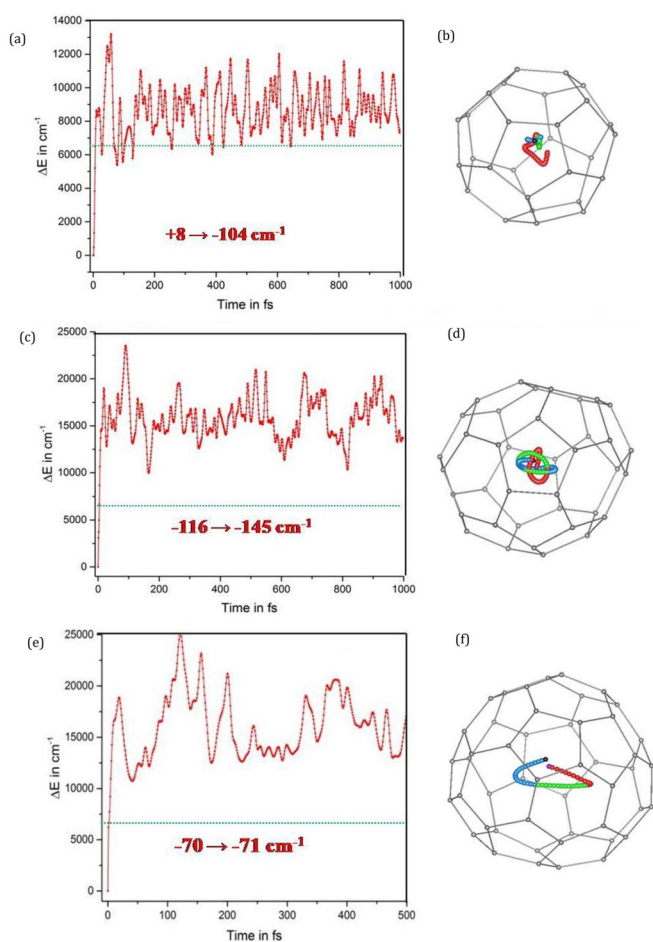


Figure 6. a), c), e) Time (in fs) evolution of energy (ΔE in cm^{-1}) for $\text{Co}@C_{28}\text{-2}$, $\text{Co}@C_{38}\text{-6}$ and $\text{Co}@C_{48}\text{-9}$ molecules, respectively. b), d), f) Trajectory of the encapsulated Co atom inside the C_{28} , C_{38} and C_{48} cages, respectively. The red, green and ocean blue regions indicated the initial, intermediate and final stages of the simulation of Co atom. Numbers in the boxes are the range of D parameters for those structures which are having energy 80 kJ mol^{-1} higher than the most stable structure.

Table 3. NEVPT2-calculated D and E/D parameters for various geometries which are close lying in energy compared to the ground state structure for $\text{Co}@C_{28}\text{-2}$, $\text{Co}@C_{38}\text{-6}$ and $\text{Co}@C_{48}\text{-9}$.

	t [fs]	ΔE [kJ mol ⁻¹]	D [cm ⁻¹]	E/D
$\text{Co}@C_{28}\text{-2}$	1	0.0	-72.9	0.00
$\text{Co}@C_{28}\text{-2}$	2	1.2	-77.1	0.00
$\text{Co}@C_{28}\text{-2}$	3	5.6	-80.6	0.00
$\text{Co}@C_{28}\text{-2}$	4	15.8	-83.3	0.00
$\text{Co}@C_{28}\text{-2}$	5	29.6	-83.6	0.00
$\text{Co}@C_{28}\text{-2}$	6	45.6	-82.8	0.01
$\text{Co}@C_{28}\text{-2}$	7	62.2	-82.6	0.01
$\text{Co}@C_{28}\text{-2}$	8	77.6	-79.7	0.01
$\text{Co}@C_{28}\text{-2}$	29	72.3	8.3	0.31
$\text{Co}@C_{28}\text{-2}$	30	74.9	8.5	0.29
$\text{Co}@C_{28}\text{-2}$	78	64.3	-15.8	0.01
$\text{Co}@C_{28}\text{-2}$	79	64.3	-18.2	0.03
$\text{Co}@C_{28}\text{-2}$	80	67.4	-21.3	0.04
$\text{Co}@C_{28}\text{-2}$	97	66.6	-52.9	0.06
$\text{Co}@C_{28}\text{-2}$	98	67.9	-55.3	0.06
$\text{Co}@C_{28}\text{-2}$	129	69.4	-118.5	0.00
$\text{Co}@C_{28}\text{-2}$	130	71.1	-104.1	0.00
$\text{Co}@C_{28}\text{-2}$	131	74.6	-85.8	0.00
<hr/>				
$\text{Co}@C_{38}\text{-6}$	1	0.0	-115.7	0.14
$\text{Co}@C_{38}\text{-6}$	2	36.9	-121.6	0.13
$\text{Co}@C_{38}\text{-6}$	3	44.4	-129.4	0.12
$\text{Co}@C_{38}\text{-6}$	4	59.4	-136.9	0.09
$\text{Co}@C_{38}\text{-6}$	5	79.9	-144.9	0.08
<hr/>				
$\text{Co}@C_{48}\text{-9}$	1	0.00	-70.1	0.04
$\text{Co}@C_{48}\text{-9}$	2	36.91	-71.4	0.04

tures are found to be low lying in energy and these are taken into consideration for computing anisotropy (see Table 3).

For $\text{Co}@C_{38}\text{-6}$ isomer with time, the ligand field geometry around Co^{II} ion is found to be the same with minor alternation in the $\text{Co}\text{-C}$ distance causing a change of D parameter by 30 cm^{-1} . For $\text{Co}@C_{48}\text{-9}$ isomer with time, the geometry around Co^{II} ion is found to be the same, resulting in almost identical anisotropy behaviour. The D and E/D value computed for $\text{Co}@C_{28}$ found to vary drastically with respect to the time with D vary from $+8.3\text{ cm}^{-1}$ (at 29 fs) to -118.5 cm^{-1} (at 129 fs). A closer look at the geometries and the orbital diagram reveal that the coordination around the Co^{II} ion is significantly altered and at 29 fs, the Co^{II} ion is four-coordinated with four carbon atoms of a pentagonal ring yielding four-legged piano-stool geometry and this then becomes three coordinated having distorted pyramidal geometry with carbon atoms of the pentagonal ring at 79 fs (see Figure S8 in the Supporting Information). At 98 fs, Co^{II} moves to the centre of a hexagonal ring and coordinates to four carbon atoms of the hexagon and one carbon atom of the adjacent $\text{C}_6\text{-C}_5\text{-C}_5$ junction, giving a highly distorted trigonal bipyramidal geometry around Co^{II} . At 130 fs the Co^{II} again becomes a three-coordinate with pyramidal structure. Between 1–8 fs, the major contribution to D comes from $d_{x^2-y^2}$ to d_{xy} transition, leading to a negative D value. At 29–30 fs, the geometry is a four-legged piano-stool geometry with no strong equatorial ligation leading to destabilisation of $d_{x^2-y^2}$ orbital and prominent transitions here are between d_{xy} to d_{xz} orbital leading to positive D value. Again at 78–80 fs, the

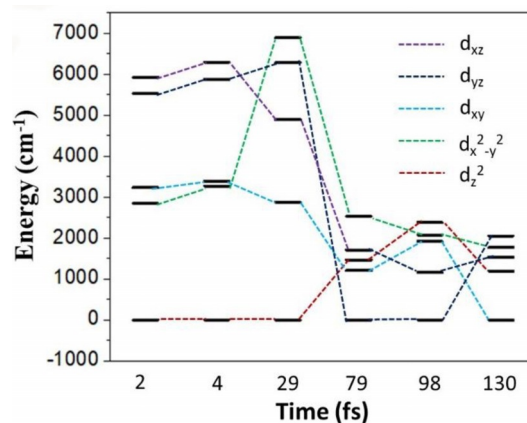


Figure 7. NEVPT2 computed d-orbitals splitting for low-lying snapshots of $\text{Co}@C_{28}\text{-2}$ cage.

geometry is distorted pyramidal and lowers overall crystal field strength. This causes contributions from both d_{xy} to $d_{x^2-y^2}/d_{xz}$ leading to small negative D value (see Figure 7 and Table S22).

Magnetic anisotropy in larger cages

Molecular dynamics studies on $\text{Co}@C_{28/38/48}$ cages suggests that as we move to larger fullerene, this yield fewer isomers which are low-lying in energy and the D values are more robust. Besides, our previous studies also suggest that enhancing the axial ligand field strength by introducing one extra bridging atom inside fullerene– $\text{Co}\text{-X}$, here X denotes oxygen or nitrogen atom (for example, $\text{CoNscZn}@C_{76/82}$ and $\text{CoOZn}@C_{70/80}$, see Figure 8), is expected to enhance the magnitude of axial anisotropy.^[8a] This incorporation of additional co-ligand inside the

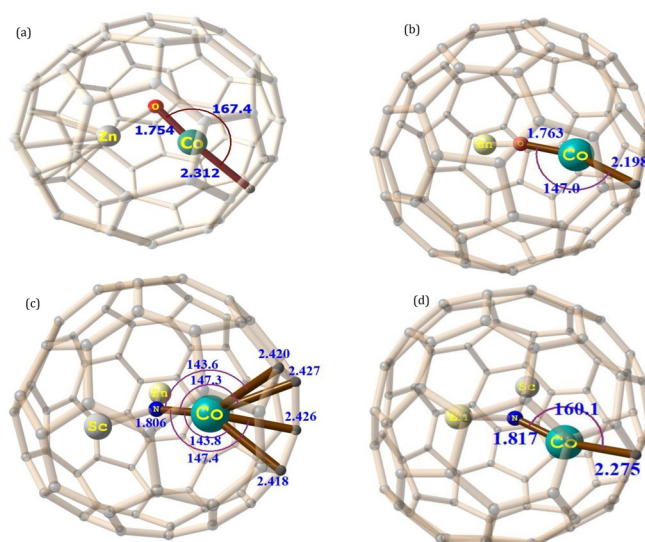


Figure 8. DFT optimised structures of a)–d) $\text{CoOZn}@C_{70}$, $\text{CoOZn}@C_{80}$, $\text{CoScZnN}@C_{76}$ and $\text{CoScZnN}@C_{82}$, respectively, with all the $\text{Co}\text{-C}$ interactions obtained from AIM analysis and with all the important structural parameters. Colour code: Co^{II} cyan green, Zn^{II} and Sc^{III} dark grey, N blue, O red and C light grey.

cage is also likely to arrest the movement of the Co^{II} ion inside the cage leading to less number of isomers and hence a robust SMMS. Experimentally several such fullerene cages are reported in the literature.^[10c,j-n,p,s,t,w]

Here we have chosen four different fullerenes namely C₇₀, C₈₀, C₇₆ and C₈₂ and inside the cage Co-O-Zn or Co-N-Sc(Zn) units are considered for our calculations. These models draw inspiration from previous reports of Sc₂O@C₈₂ and V_xSc_{3-x}N@C₈₀ (x = 1, 2).^[10c,20] The computed *D*, *E/D* and *g*-tensors are listed in Table 4.

Models	<i>D</i> [cm ⁻¹]	<i>E/D</i>	<i>g</i> _{xx} , <i>g</i> _{yy} , <i>g</i> _{zz}
CoOZn@C ₇₀	-184.6	0.01	1.41, 1.66, 4.28
CoOZn@C ₈₀	-148.1	0.03	1.94, 2.23, 3.72
CoZnScN@C ₇₆	-141.2	0.01	1.22, 1.80, 3.70
CoZnScN@C ₈₂	-150.1	0.04	1.86, 2.18, 3.72

SA-CASSCF calculation on these four cages yields a very high negative *D* values (see Table 4). The dominant ground state electronic arrangement for cages CoOZn@C₇₀, CoOZn@C₈₀, CoScZnN@C₇₆ and CoScZnN@C₈₂ is found to be (d_{z²})²(d_{xy})¹(d_{xz})²(d_{x²-y²})¹(d_{yz})¹, (d_{yz})¹(d_{x²-y²})²(d_{xz})²(d_{xy})¹(d_{z²})¹, (d_{z²})¹(d_{x²-y²})²(d_{xz})²(d_{xy})¹(d_{yz})¹ and (d_{xy})¹(d_{x²-y²})²(d_{xz})¹(d_{z²})¹(d_{yz})² with 37%, 27%, 42% and 26% contributions, respectively. In these isomers, the largest contribution to *D* comes from d_{xy/x²-y²} → d_{x²-y²/xy} and d_{xz/yz} → d_{yz/xz} transitions (see Figure 9 and Table S23). The magnitude of *D* can be explained based on the energy separation between orbitals and this orbital ordering is strongly correlated to the geometry around Co^{II} ion in the cage. Smaller the energy separation between these orbitals, larger will be the magnitude of *D* and vice versa (see Figure 10). For cage CoOZn@C₇₀, the computed *D* value is found to be -184.6 cm⁻¹, one of the highest value predicted for any Co^{II} complexes.^[21] As discussed earlier, the very small *E* parameter is the outcome of the comparable transitions between both d_{x²-y²/xy} → d_{xz/yz} and d_{x²-y²/xy} → d_{xy/x²-y²} or d_{xz/yz} → d_{yz/xz} (see Figure 9, Table S24–27). As the symmetry around the metal ion is found to be higher for all these four cages, the *E/D* parameter is found to be small or negligible (<0.05) emphasising the potential of these molecules to exhibit SIM characteristics.

As discussed previously, for larger endohedral fullerenes, the isomers generated are relatively higher in energy and are thus unlikely to be accessible and this is also true for the four models discussed (CoNScZn@C_{76/82} and CoOZn@C_{70/80}). This is due to the fact that breaking of multiple M–C(fullerene) bonds (Co–C, Zn–C and Sc–C) required to attain other isomers and the energy penalty associated with this step is very steep for these structures as revealed by the very large formation energies computed (formation energy of -1891 kJ mol⁻¹, -1729 kJ mol⁻¹, -5881 kJ mol⁻¹ and -5819 kJ mol⁻¹, respectively for CoOZn@C₇₀, CoOZn@C₈₀, CoScZnN@C₇₆ and CoScZnN@C₈₂ cages). AIM analysis suggests a two-coordinate

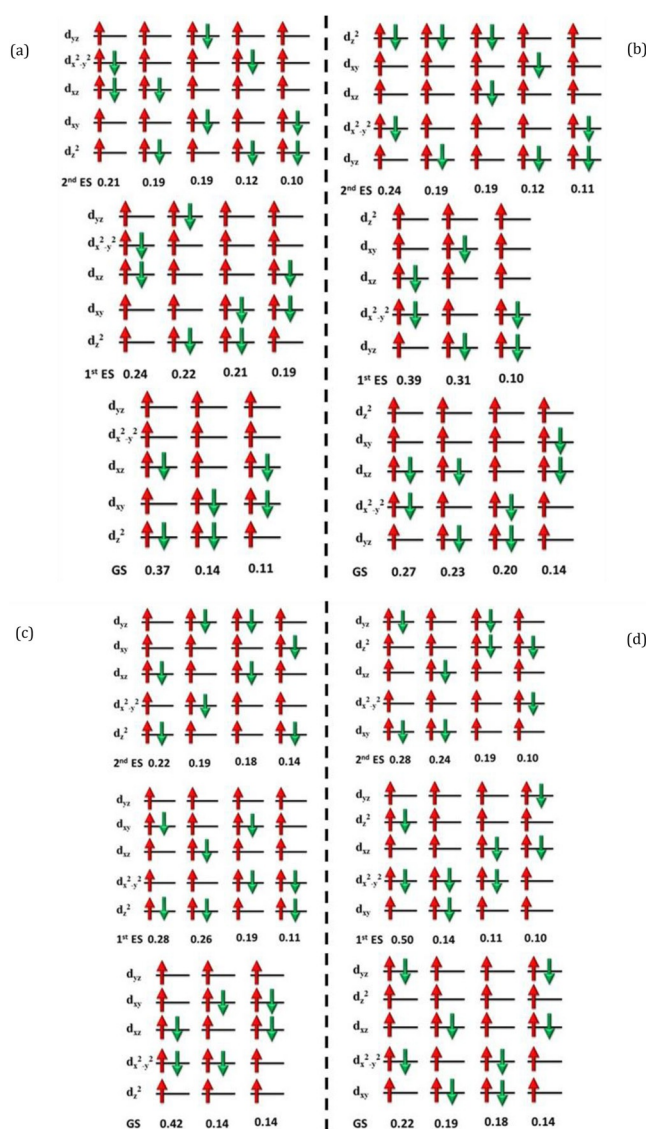


Figure 9. Multi-determinant wavefunction of the ground and excited states for a) CoOZn@C₇₀, b) CoOZn@C₈₀, c) CoScZnN@C₇₆ and d) CoScZnN@C₈₂ EMFs. The computed CI coefficients that are larger than 10% are shown above.

linear geometry around Co^{II} ion for CoOZn@C_{70/80} and CoScZnN@C₈₂ cages. Whereas for CoScZnN@C₇₆, the geometry around Co^{II} is found to be five-coordinate distorted square-pyramidal (see Figure S9 and Table S28). Linearity around Co^{II} is found to be more for CoOZn@C₇₀ than for the CoScZnN@C₈₂ cage and this is followed by CoOZn@C₈₀ cage. This explains the observed trend of the anisotropy among these four models.

Conclusions

To this end, our theoretical search for a large magnetic anisotropic system leads us to Co^{II} ion/cluster encapsulated fullerenes, where extremely large axial anisotropy is predicted. Strong axial ligand field in the presence of a weak transverse field around paramagnetic Co^{II} ion provides a molecular

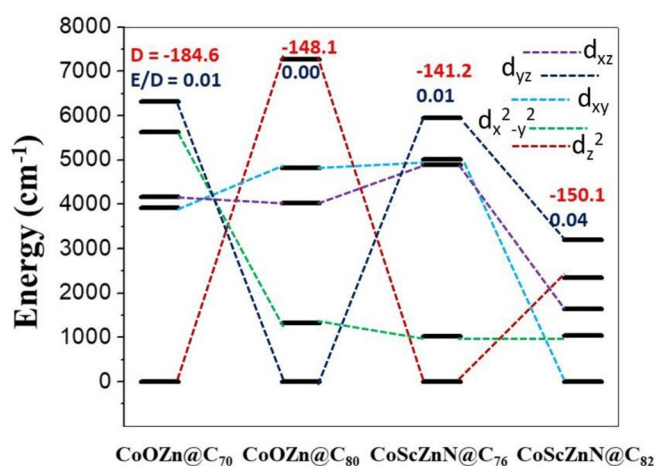


Figure 10. SA-CASSCF computed d-orbitals splitting for CoOZn@C₇₀, CoOZn@C₈₀, CoScZnN@C₇₆ and CoScZnN@C₈₂ cages. The values written above the diagrams are computed D (red) and E/D (dark blue) values.

system with low coordination number which is difficult to achieve in traditional coordination complexes. Moreover, high anisotropy, high-symmetry, no-nuclear spin atoms such as H, high-rigidity due to strong carbon-carbon bond are expected to quench other possible relaxation processes to yield robust SMMs. Major findings from this study can be summarised below.

- 1) We begin with modelling Co@C₂₈, C₃₈ and C₄₈ cages and their isomers for potential target molecules that could yield very large magnetic anisotropy. Modelling encompasses determining lower energy structure among various isomers using density functional methods and later employ lower energy structure to compute magnetic anisotropy D and E using CASSCF/NEVPT2 methods. Further, we have also performed molecular dynamics using DFT methods to estimate various conformational geometries that are energetically accessible and utilised again CASSCF/NEVPT2 method to estimate D and E on these conformational snapshots to see how robust the estimated parameters are. This theoretical methodology unveiled here is a combination of DFT/CASSCF/MD methods to screen potential targets for superior SMMs and attempt has been made to take into consideration various factors that facilitate relaxation of magnetisation process and not simply the D and E parameters of the ground state structure.
- 2) Our calculations reveal that in C₂₈ cage tested, the D values vary significantly between two isomers that are considered (from $D = -24.3 \text{ cm}^{-1}$ to -72.4 cm^{-1}). While NBO and AIM analysis reveals rather strong Co–C bonds in these cages, the worrying feature is revealed in molecular dynamics simulation where the energy required to move Co^{II} ion within the cage is found to be small and hence the Co^{II} is expected to freely rotate inside the cage generating large conformational geometries at higher temperatures. Computing D and E values for these conformational snapshots reveal significant variation in D (from $+8 \text{ cm}^{-1}$ to -104 cm^{-1}). De-

spite the fact that the energetically low lying isomer of C₂₈ cage has robust D value, accessibility to the various conformations some of which even possess a positive D value likely to facilitate relaxation of magnetisation that is not purely governed by Orbach process and hence may not yield attractive blocking temperatures. For Co@C₃₈ and Co@C₄₈ cages as well the D values are found to vary significantly with the different isomers; however, the movement of the Co^{II} ion in these cages causes significant energy penalty leading to a few conformational snapshots. Particularly Co@C₄₈ cages seem attractive as they yield very large D and small E/D values and also found to possess only a few conformational snapshots where D and E/D parameters are nearly invariant.

- 3) Further suggestion to arrest the movement and to enhance the axially was considered by modelling various coordination motifs that contain Co^{II} ions inside fullerenes. These include models such as CoOZn@C₇₀, CoOZn@C₈₀, CoScZnN@C₇₆ and CoScZnN@C₈₂. Here due to strong binding of Co^{II} to oxygen or nitrogen atom, which is connected to another diamagnetic transition metal ion, strong axially was witnessed leading to extremely large D values. For CoOZn@C₇₀ model D values as high as $\approx -200 \text{ cm}^{-1}$ with negligible E/D values are predicted. Formation energies and MD performed on other molecules reveal that the units incorporated inside the fullerene cage are very robust and likely to yield an attractive barrier for magnetisation reversal. Earlier reports on the X-ray structures of V_xSc_{3-x}N@C₈₀ ($x = 1, 2$) suggest that these predictions are synthetically viable.

Encouraged by the fact that our earlier predictions on Ln₂@C₇₉N and DyODy@C₈₂ cages have been proved, here we set out to undertake a comprehensive study on Co^{II} endohedral fullerenes with an aim to set a target for superior SMMs which are also stable under ambient conditions.

Computational Details

Estimating Magnetic Anisotropy

Reaction The spin-Hamiltonian which determines the zero-field splitting parameter for transition metal complexes is given by Equation (1).

$$\hat{H}_{ZFS} = D \left[\hat{S}_z^2 - S(S+1)/3 \right] + E \left(\hat{S}_x^2 - \hat{S}_y^2 \right) \quad (1)$$

Here D and E are the axial zero-field splitting parameter and rhombic zero-field splitting parameter; and S , S_x , S_y and S_z are the total spin toward its x , y and z components, respectively. The overall D , which is a tensor quantity and its components for the diagonalised and traceless condition can be expressed by Equation (2).

$$D = D_{zz} - \frac{1}{2}(D_{xx} + D_{yy}); \quad E = \frac{1}{2}(D_{xx} - D_{yy}) \quad (2)$$

The components of D (say, D_{ij} in general) are itself negative by the equation derived from second-order perturbation theory given by Equation (3).^[11c,d]

$$D_{ij} = -\frac{\zeta^2}{4S^2} \sum_{p,q} \frac{\langle \psi_p | \hat{l}_i | \psi_q \rangle \langle \psi_q | \hat{l}_j | \psi_p \rangle}{\varepsilon_q - \varepsilon_p} - \frac{\zeta^2}{4S^2} \sum_{r,q} \frac{\langle \psi_q | \hat{l}_i | \psi_r \rangle \langle \psi_r | \hat{l}_j | \psi_q \rangle}{\varepsilon_r - \varepsilon_q} \quad (3)$$

Here, ζ^2 is the effective spin-orbit coupling constant of the molecule, ψ_p , ψ_q and ψ_r are the doubly occupied, singly occupied and vacant molecular orbitals, respectively. ε is the orbital energy. The first term corresponds to $\beta \rightarrow \beta$ (spin-allowed) electronic transition and the second term corresponds to $\alpha \rightarrow \alpha$ (spin-allowed) electronic transition. In addition, l_i and l_j are the x , y or z components of the total orbital angular momentum operator L , which connects the corresponding ground state wavefunction with the excited state. The D parameter is negative when $D_{ZZ} > (D_{XX} + D_{YY})$ and vice versa. Electronic transitions within the same m_l levels result in dominant D_{ZZ} term as shown in Equation (3).^[7d]

The \mathbf{g} -tensors and the zero-field splitting parameters were computed using the ab initio NEVPT2 method as implemented in the ORCA software suite.^[22] Ab initio calculations generally yield a good estimate of anisotropy compared to density functional methods, as it has been shown recently.^[23] State-average CASSCF calculations were performed for Co^{II} ions incorporating the five d-orbitals and seven electrons in the active space (CAS (7,5) setup). Calculations were carried out with ten quartets and forty doublet excited states in our calculations.^[23e] Here, we employed def2-TZVPP basis set for Co^{II} and def2-TZVP basis set for the Sc, Zn, O, N and C.^[24] The calculations utilised the RI approximation with the auxiliary def2-SVP/C and def2-SV/C Coulomb fitting basis sets and the chain-of spheres (RI-COSX) approximation. The employed methodology was used earlier to obtain an accurate estimation of the zero-field splitting (zfs) parameters.^[7b,d,23b,25] To treat the dynamic correlations, N-electron valence perturbation theory (NEVPT2) calculations^[26] on SA-CASSCF converged wave functions were performed. Since the NEVPT2 correlated energies are found to be more accurate towards the estimation of zfs parameters,^[23b,25a-c,e] here we have restricted our analysis to NEVPT2 results. The reported \mathbf{g} -tensors were also computed using the same methodology. The zero-field splitting parameters were extracted using the effective Hamiltonian approach (EHA) that has been shown in several cases to yield good numerical estimate of this parameter.^[7]

Molecular dynamics using DFT

To check the effect of dynamics on magnetic anisotropy, we carried out ab initio molecular dynamics (AIMD) using the atom-centred density matrix propagation (ADMP) technique^[27] as implemented in the G09 suite of programme, using UB3LYP level^[28] with a 6-31G* basis set^[29] for carbon, nitrogen, oxygen atoms and LanL2DZ, which encompasses a double- ζ quality basis set with the Los Alamos effective core potential, for

Co.^[30] Boltzmann distribution was used to generate the initial nuclear kinetic energies. The temperature was maintained by using a velocity scaling thermostat throughout the simulation. All the simulations were carried out at 300 K. Default random number generator seed was used, as implemented in Gaussian 09 to initiate the initial mass-weighted Cartesian velocity. For all the cases, trajectories up to 1000 femtosecond (fs) were generated. We performed AIMD on the lowest stable structure of all the studied fullerenes at 300 K.^[31]

Structure and bonding using DFT methods

All structures optimisation were performed using G09 suite of the program using density functional theory (DFT).^[32] For the chosen fullerene cages various isomers are possible. To include this effect in our calculations, we have chosen various isomers which are close lying in energy. The isomers initial geometries were obtained from <http://www.nanotube.msu.edu/> and were then optimised at the UB3LYP level^[28] with a 6-31G* basis set^[29] for carbon, nitrogen, oxygen atoms and LanL2DZ, which encompasses a double- ζ quality basis set with the Los Alamos effective core potential, for Co, Sc, Zn atoms.^[30] Various isomers within the cages are denoted as C_n - \mathbf{M} with n being various fullerene cages (28, 38 and 48 for example) and \mathbf{M} being the isomer number. The geometries of all isomers are given in Supporting Information and, their description and APR numbers are given in Table 1 and text below. To estimate the energetics, single-point calculations were performed on the optimised structures using TZV basis set for all atoms.^[33] These energetics were used to determine the ground-state structure and the lowest energy isomers among various Co@ C_n cages. There have been many instances in which several energetically high-lying isomers (as high as for example 63 kJ mol⁻¹, $Sc_2C_2@C_{80}$)^[34] of fullerene have been synthesised and characterised. Here, we have taken 80 kJ mol⁻¹ as a ball-park number to assess various isomers to be included in the set of structures for which anisotropy can be analysed. Additionally, to probe the bonding further, atoms in molecule (AIM) analysis was performed to determine the nature of the Co–C interaction and how this is correlated to the magnetic anisotropy (see Supporting Information for further details). Thus, within the framework of the AIM theory, the related AIM parameters such as bond critical points (BCPs) have been computed to gain insight into the bonding.^[35]

Acknowledgements

G.R. would like to acknowledge the financial support from SERB-DST (CRG/2018/000430) India, and IIT Bombay for the high-performance computing facility. M.K.S., P.S. and M.K. would like to thank IIT Bombay for financial assistance.

Conflict of interest

The authors declare no conflict of interest.

Keywords: anisotropy · cobalt · endohedral fullerene · molecular dynamics · single molecule magnets

- [1] a) J. Zhang, W. Kosaka, K. Sugimoto, H. Miyasaka, *J. Am. Chem. Soc.* **2018**, *140*, 5644–5652; b) J. Yuan, S.-Q. Wu, M.-J. Liu, O. Sato, H.-Z. Kou, *J. Am. Chem. Soc.* **2018**, *140*, 9426–9433; c) T. Yamabayashi, M. Atzori, L. Tesi, G. Cosquer, F. Santanni, M.-E. Boulon, E. Morra, S. Benci, R. Torre, M. Chiesa, L. Sorace, R. Sessoli, M. Yamashita, *J. Am. Chem. Soc.* **2018**, *140*, 12090–12101; d) Y.-X. Wang, Y. Ma, Y. Chai, W. Shi, Y. Sun, P. Cheng, *J. Am. Chem. Soc.* **2018**, *140*, 7795–7798; e) W. Wang, C. Chen, C. Shu, S. Rajca, X. Wang, A. Rajca, *J. Am. Chem. Soc.* **2018**, *140*, 7820–7826; f) B. W. Stein, C. R. Tichnell, J. Chen, D. A. Shultz, M. L. Kirk, *J. Am. Chem. Soc.* **2018**, *140*, 2221–2228; g) T. Morita, M. Damjanović, K. Katoh, Y. Kitagawa, N. Yasuda, Y. Lan, W. Wernsdorfer, B. K. Breedlove, M. Enders, M. Yamashita, *J. Am. Chem. Soc.* **2018**, *140*, 2995–3007; h) M. Magott, M. Reczyński, B. Gawel, B. Sieklucka, D. Pinkowicz, *J. Am. Chem. Soc.* **2018**, *140*, 15876–15882; i) C. Lochenie, K. Schötz, F. Panzer, H. Kurz, B. Maier, F. Puchler, S. Agarwal, A. Köhler, B. Weber, *J. Am. Chem. Soc.* **2018**, *140*, 700–709; j) M.-J. Liu, J. Yuan, J. Tao, Y.-Q. Zhang, C.-M. Liu, H.-Z. Kou, *Inorg. Chem.* **2018**, *57*, 4061–4069; k) Z. Hu, B.-W. Dong, Z. Liu, J.-J. Liu, J. Su, C. Yu, J. Xiong, D.-E. Shi, Y. Wang, B.-W. Wang, A. Ardavan, Z. Shi, S.-D. Jiang, S. Gao, *J. Am. Chem. Soc.* **2018**, *140*, 1123–1130; l) X. Li, J. Yang, *J. Am. Chem. Soc.* **2019**, *141*, 109–112; m) R. Hussain, G. Allodi, A. Chiesa, E. Garlatti, D. Mitcov, A. Konstantatos, K. S. Pedersen, R. De Renzi, S. Piligkos, S. Carretta, *J. Am. Chem. Soc.* **2018**, *140*, 9814–9818; n) C. Huang, J. Feng, F. Wu, D. Ahmed, B. Huang, H. Xiang, K. Deng, E. Kan, *J. Am. Chem. Soc.* **2018**, *140*, 11519–11525; o) J.-K. Bao, Z.-T. Tang, H. J. Jung, J.-Y. Liu, Y. Liu, L. Li, Y.-K. Li, Z.-A. Xu, C.-M. Feng, H. Chen, D. Y. Chung, V. P. Dravid, G.-H. Cao, M. G. Kanatzidis, *J. Am. Chem. Soc.* **2018**, *140*, 4391–4400; p) B. S. Dolinar, D. I. Alexandropoulos, K. R. Vignesh, T. A. James, K. R. Dunbar, *J. Am. Chem. Soc.* **2018**, *140*, 908–911; q) T. Delgado, A. Tissot, L. Guéneé, A. Hauser, F. J. Valverde-Muñoz, M. Sereidyuk, J. A. Real, S. Pillet, E.-E. Bendeif, C. Besnard, *J. Am. Chem. Soc.* **2018**, *140*, 12870–12876; r) K. Chakarawet, P. C. Bunting, J. R. Long, *J. Am. Chem. Soc.* **2018**, *140*, 2058–2061; s) B. S. Billow, B. N. Livesay, C. C. Mokhtarzadeh, J. McCracken, M. P. Shores, J. M. Boncella, A. L. Odom, *J. Am. Chem. Soc.* **2018**, *140*, 17369–17373; t) Y. Zhou, X.-Y. Zheng, J. Cai, Z.-F. Hong, Z.-H. Yan, X.-J. Kong, Y.-P. Ren, L.-S. Long, L.-S. Zheng, *Inorg. Chem.* **2017**, *56*, 2037–2041; u) F.-S. Guo, B. M. Day, Y.-C. Chen, M.-L. Tong, A. Mansikkamäki, R. A. Layfield, *Science* **2018**, *362*, 1400–1403; v) K. Randall McClain, C. A. Gould, K. Chakarawet, S. J. Teat, T. J. Groshens, J. R. Long, B. G. Harvey, *Chem. Sci.* **2018**, *9*, 8492–8503; w) G. A. Craig, A. Sarkar, C. H. Woodall, M. A. Hay, K. E. R. Marriott, K. V. Kamenev, S. A. Moggach, E. K. Brechin, S. Parsons, G. Rajaraman, M. Murrie, *Chem. Sci.* **2018**, *9*, 1551–1559; x) C. H. Chen, D. S. Krylov, S. M. Avdoshenko, F. Liu, L. Spree, R. Yadav, A. Alvertis, L. Hozoi, K. Nenkov, A. Kostanyan, T. Greber, A. U. B. Wolter, A. A. Popov, *Chem. Sci.* **2017**, *8*, 6451–6465; y) L. Escalera-Moreno, J. J. Baldovi, A. Gaita-Arino, E. Coronado, *Chem. Sci.* **2018**, *9*, 3265–3275; z) Y. Z. Zhang, B. S. Dolinar, S. Liu, A. J. Brown, X. Zhang, Z. X. Wang, K. R. Dunbar, *Chem. Sci.* **2018**, *9*, 119–124; aa) K. A. Schulte, K. R. Vignesh, K. R. Dunbar, *Chem. Sci.* **2018**, *9*, 9018–9026; ab) C. A. P. Goodwin, F. Ortu, D. Reta, N. F. Chilton, D. P. Mills, *Nature* **2017**, *548*, 439–442.
- [2] S. A. Corrales, J. M. Cain, K. A. Uhlig, A. M. Mowson, C. Papatrifiantylopoulou, M. K. Peprah, A. Ozarowski, A. J. Tasiopoulos, G. Christou, M. W. Meisel, C. Lampropoulos, *Inorg. Chem.* **2016**, *55*, 1367–1369.
- [3] a) A. Caneschi, D. Gatteschi, R. Sessoli, A. L. Barra, L. C. Brunel, M. Guillot, *J. Am. Chem. Soc.* **1991**, *113*, 5873–5874; b) R. Sessoli, D. Gatteschi, A. Caneschi, M. A. Novak, *Nature* **1993**, *365*, 141–143; c) L. Thomas, F. Lioni, R. Ballou, D. Gatteschi, R. Sessoli, B. Barbara, *Nature* **1996**, *383*, 145; d) W. Wernsdorfer, R. Sessoli, *Science* **1999**, *284*, 133–135; e) D. Gatteschi, A. Caneschi, L. Pardi, R. Sessoli, *Science* **1994**, *265*, 1054–1058; f) M. N. Leuenberger, D. Loss, *Nature* **2001**, *410*, 789–793; g) S. Hill, R. S. Edwards, N. Aliaga-Alcalde, G. Christou, *Science* **2003**, *302*, 1015–1018; h) R. E. P. Winpenny, *Angew. Chem. Int. Ed.* **2008**, *47*, 7992–7994; *Angew. Chem.* **2008**, *120*, 8112–8114; i) M. Affronte, F. Troiani, A. Ghirri, A. Candini, M. Evangelisti, V. Corradini, S. Carretta, P. Santini, G. Amoretti, F. Tuna, G. Timco, R. E. P. Winpenny, *J. Phys. D* **2007**, *40*, 2999–3004; j) F. Troiani, *Phys. Rev. Lett.* **2005**, *94*, 207208; k) F. K. Larsen, E. J. L. McInnes, H. E. Mkami, J. Overgaard, S. Piligkos, G. Rajaraman, E. Rentzschler, A. A. Smith, G. M. Smith, V. Boote, M. Jennings, G. A. Timco, R. E. P. Winpenny, *Angew. Chem. Int. Ed.* **2003**, *42*, 101–105; *Angew. Chem.* **2003**, *115*, 105–109; l) I. Bogani, W. Wernsdorfer, *Nat. Mater.* **2008**, *7*, 179–186; m) S. Sanvito, *Chem. Soc. Rev.* **2011**, *40*, 3336–3355.
- [4] a) C. J. Milios, A. Vinslava, W. Wernsdorfer, S. Moggach, S. Parsons, S. P. Perlepes, G. Christou, E. K. Brechin, *J. Am. Chem. Soc.* **2007**, *129*, 2754–2755; b) C. J. Milios, R. Inglis, A. Vinslava, R. Bagai, W. Wernsdorfer, S. Parsons, S. P. Perlepes, G. Christou, E. K. Brechin, *J. Am. Chem. Soc.* **2007**, *129*, 12505–12511; c) C. J. Milios, A. Vinslava, W. Wernsdorfer, A. Prescimone, P. A. Wood, S. Parsons, S. P. Perlepes, G. Christou, E. K. Brechin, *J. Am. Chem. Soc.* **2007**, *129*, 6547–6561.
- [5] J. M. Zadrozny, D. J. Xiao, M. Atanasov, G. J. Long, F. Grandjean, F. Neese, J. R. Long, *Nat. Chem.* **2013**, *5*, 577–581.
- [6] a) P. H. Lin, T. J. Burchell, L. Unger, L. F. Chibotaru, W. Wernsdorfer, M. Murugesu, *Angew. Chem. Int. Ed.* **2009**, *48*, 9489–9492; *Angew. Chem.* **2009**, *121*, 9653–9656; b) S. K. Gupta, T. Rajeshkumar, G. Rajaraman, R. Murugavel, *Chem. Sci.* **2016**, *7*, 5181–5191; c) T. Gupta, M. K. Singh, G. Rajaraman, in *Organometallic Magnets*, Springer, **2018**; d) N. Rösch, O. D. Häberlen, B. I. Dunlap, *Angew. Chem. Int. Ed. Engl.* **1993**, *32*, 108–110; *Angew. Chem.* **1993**, *105*, 78–81.
- [7] a) R. Ruamps, R. Maurice, L. Batchelor, M. Boggio-Pasqua, R. Guillot, A. L. Barra, J. Liu, E.-E. Bendeif, S. Pillet, S. Hill, T. Mallah, N. Guihéry, *J. Am. Chem. Soc.* **2013**, *135*, 3017–3026; b) R. Maurice, C. de Graaf, N. Guihéry, *Phys. Chem. Chem. Phys.* **2013**, *15*, 18784–18804; c) R. Maurice, N. Guihéry, R. Bastardis, C. de Graaf, *J. Chem. Theory Comput.* **2010**, *6*, 55–65; d) R. Maurice, R. Bastardis, C. de Graaf, N. Suaud, T. Mallah, N. Guihéry, *J. Chem. Theory Comput.* **2009**, *5*, 2977–2984; e) L. Ungur, L. F. Chibotaru, *The computer programs SINGLE ANISO and POLY ANISO*, University of Leuven, **2006**.
- [8] a) M. K. Singh, G. Rajaraman, *Chem. Commun.* **2016**, *52*, 14047–14050; b) M. K. Singh, N. Yadav, G. Rajaraman, *Chem. Commun.* **2015**, *51*, 17732–17735.
- [9] T. Gupta, M. F. Beg, G. Rajaraman, *Inorg. Chem.* **2016**, *55*, 11201–11215.
- [10] a) F. Liu, D. S. Krylov, L. Spree, S. M. Avdoshenko, N. A. Samoylova, M. Rosenkranz, A. Kostanyan, T. Greber, A. U. B. Wolter, B. Buchner, A. A. Popov, *Nat. Commun.* **2017**, *8*, 16098; b) S. Zhou, M. Yamamoto, G. A. D. Briggs, H. Imahori, K. Porfyrikis, *J. Am. Chem. Soc.* **2016**, *138*, 1313–1319; c) T. Wei, S. Wang, X. Lu, Y. Tan, J. Huang, F. Liu, Q. Li, S. Xie, S. Yang, *J. Am. Chem. Soc.* **2016**, *138*, 207–214; d) Y. Hashikawa, M. Murata, A. Wakamiya, Y. Murata, *J. Am. Chem. Soc.* **2016**, *138*, 4096–4104; e) Y. Takano, R. Tashita, M. Suzuki, S. Nagase, H. Imahori, T. Akasaka, *J. Am. Chem. Soc.* **2016**, *138*, 8000–8006; f) Y. Hashikawa, M. Murata, A. Wakamiya, Y. Murata, *Angew. Chem. Int. Ed.* **2016**, *55*, 13109–13113; *Angew. Chem.* **2016**, *128*, 13303–13307; g) L. Bao, C. Pan, Z. Slanina, F. Uhlík, T. Akasaka, X. Lu, *Angew. Chem. Int. Ed.* **2016**, *55*, 9234–9238; *Angew. Chem.* **2016**, *128*, 9380–9384; h) L. Bao, M. Chen, C. Pan, T. Yamaguchi, T. Kato, M. M. Olmstead, A. L. Balch, T. Akasaka, X. Lu, *Angew. Chem. Int. Ed.* **2016**, *55*, 4242–4246; *Angew. Chem.* **2016**, *128*, 4314–4318; i) Z. Wang, S. Aoyagi, H. Omachi, R. Kitaura, H. Shinohara, *Angew. Chem. Int. Ed.* **2016**, *55*, 199–202; *Angew. Chem.* **2016**, *128*, 207–210; j) K. Junghans, K. B. Ghiassi, N. A. Samoylova, Q. Deng, M. Rosenkranz, M. M. Olmstead, A. L. Balch, A. A. Popov, *Chem. Eur. J.* **2016**, *22*, 13098–13107; k) C.-H. Chen, L. Abella, M. R. Cerón, M. A. Guerrero-Ayala, A. Rodríguez-Fortea, M. M. Olmstead, X. B. Powers, A. L. Balch, J. M. Poblet, L. Echegoyen, *J. Am. Chem. Soc.* **2016**, *138*, 13030–13037; l) W. Cai, F.-F. Li, L. Bao, Y. Xie, X. Lu, *J. Am. Chem. Soc.* **2016**, *138*, 6670–6675; m) W.-J. Guan, P. Zhao, Q.-Z. Li, S. Nagase, M. Ehara, X. Zhao, *RSC Adv.* **2016**, *6*, 75588–75593; n) P. Zhao, J.-S. Dang, X. Zhao, *Phys. Chem. Chem. Phys.* **2016**, *18*, 9709–9714; o) S. Mamone, M. R. Johnson, J. Ollivier, S. Rols, M. H. Levitt, A. J. Horsewill, *Phys. Chem. Chem. Phys.* **2016**, *18*, 1998–2005; p) M. R. Cerón, M. Izquierdo, N. Alegret, J. A. Valdez, A. Rodríguez-Fortea, M. M. Olmstead, A. L. Balch, J. M. Poblet, L. Echegoyen, *Chem. Commun.* **2016**, *52*, 64–67; q) S. A. Tawfik, X. Y. Cui, S. P. Ringer, C. Stampf, *Phys. Chem. Chem. Phys.* **2016**, *18*, 21315–21321; r) A. K. Srivastava, S. K. Pandey, N. Misra, *Mater. Res. Express* **2016**, *3*, 04508–04513; s) K. Junghans, C. Schlesier, A. Kostanyan, N. A. Samoylova, Q. Deng, M. Rosenkranz, S. Schiemenz, R. Westerström, T. Greber, B. Büchner, A. A. Popov, *Angew. Chem. Int. Ed.* **2015**, *54*, 13411–13415; *Angew. Chem.* **2015**, *127*, 13609–13613; t) T. Yang, Y. Hao, L. Abella, Q. Tang, X. Li, Y. Wan, A. Rodríguez-Fortea, J. M. Poblet, L. Feng, N. Chen, *Chem. Eur. J.*

- 2015, 21, 11110–11117; u) N. Okamura, K. Yoshida, S. Sakata, K. Hirakawa, *Appl. Phys. Lett.* **2015**, 106, 043108–043111; v) S. F. Yang, C. R. Wang, *Endohedral Fullerenes: From Fundamentals to Applications*, World Scientific, <https://doi.org/10.1142/8785>, **2014**; w) J. Dreiser, R. Westerström, Y. Zhang, A. A. Popov, L. Dunsch, K. Krämer, S.-X. Liu, S. Decurtins, T. Greber, *Chem. Eur. J.* **2014**, 20, 13536–13540.
- [11] a) S. Vaidya, S. Tewary, S. K. Singh, S. K. Langley, K. S. Murray, Y. Lan, W. Wernsdorfer, G. Rajaraman, M. Shanmugam, *Inorg. Chem.* **2016**, 55, 9564–9578; b) J. Cirera, E. Ruiz, S. Alvarez, F. Neese, J. Kortus, *Chem. Eur. J.* **2009**, 15, 4078–4087; c) S. Gómez-Coca, E. Cremades, N. Aliaga-Alcalde, E. Ruiz, *Inorg. Chem.* **2014**, 53, 676–678; d) S. Gómez-Coca, D. Aravena, R. Morales, E. Ruiz, *Coord. Chem. Rev.* **2015**, 289–290, 379–392; e) J. Caballero-Jiménez, F. Habib, D. Ramírez-Rosales, R. Grande-Aztatzi, G. Merino, I. Korobkov, M. K. Singh, G. Rajaraman, Y. Reyes-Ortega, M. Murugesu, *Dalton Trans.* **2015**, 44, 8649–8659; f) S. K. Singh, T. Gupta, P. Badkur, G. Rajaraman, *Chem. Eur. J.* **2014**, 20, 10305–10313.
- [12] P. C. Bunting, M. Atanasov, E. Damgaard-Møller, M. Perfetti, I. Crassee, M. Orlita, J. Overgaard, J. van Slageren, F. Neese, J. R. Long, *Science* **2018**, 362, eaat7319.
- [13] a) J. M. Zadrozny, J. R. Long, *J. Am. Chem. Soc.* **2011**, 133, 20732–20734; b) S. Gomez-Coca, E. Cremades, N. Aliaga-Alcalde, E. Ruiz, *J. Am. Chem. Soc.* **2013**, 135, 7010–7018; c) Y. Rechkemmer, F. D. Breitgoff, M. van der Meer, M. Atanasov, M. Hakl, M. Orlita, P. Neugebauer, F. Neese, B. Sarkar, J. van Slageren, *Nat. Commun.* **2016**, 7, 10467; d) M. S. Fataftah, J. M. Zadrozny, D. M. Rogers, D. E. Freedman, *Inorg. Chem.* **2014**, 53, 10716–10721; e) C. Y. Lin, J. D. Guo, J. C. Fettinger, S. Nagase, F. Grandjean, G. J. Long, N. F. Chilton, P. P. Power, *Inorg. Chem.* **2013**, 52, 13584–13593; f) I. G. Rau, S. Baumann, S. Rusponi, F. Donati, S. Stepanow, L. Gragnaniello, J. Dreiser, C. Piamonteze, F. Nolting, S. Gangopadhyay, *Science* **2014**, 344, 988–992.
- [14] S. K. Singh, G. Rajaraman, *Nat. Commun.* **2016**, 7, 10669.
- [15] a) P. W. Dunk, N. K. Kaiser, M. Mulet-Gas, A. Rodríguez-Forteza, J. M. Poblet, H. Shinohara, C. L. Hendrickson, A. G. Marshall, H. W. Kroto, *J. Am. Chem. Soc.* **2012**, 134, 9380–9389; b) M. Mulet-Gas, L. Abella, P. W. Dunk, A. Rodríguez-Forteza, H. W. Kroto, J. M. Poblet, *Chem. Sci.* **2015**, 6, 675–686.
- [16] P. W. Fowler, *Contemp. Phys.* **1996**, 37, 235–247.
- [17] a) X. N. Yao, J. Z. Du, Y. Q. Zhang, X. B. Leng, M. W. Yang, S. D. Jiang, Z. X. Wang, Z. W. Ouyang, L. Deng, B. W. Wang, S. Gao, *J. Am. Chem. Soc.* **2017**, 139, 373–380; b) S. Vaidya, A. Upadhyay, S. K. Singh, T. Gupta, S. Tewary, S. K. Langley, J. P. S. Walsh, K. S. Murray, G. Rajaraman, M. Shanmugam, *Chem. Commun.* **2015**, 51, 3739–3742.
- [18] F. Neese, E. I. Solomon, *Magnetism: Molecules to Materials* **2004**, Wiley-VCH, Weinheim.
- [19] We have performed NEVPT2 calculations for Co@C_{28/38/48} (except Co@C₃₈-5) cages and for other larger models we have analysed SA-CASSCF because of large computational demands and non-convergence.
- [20] Q. Tang, L. Abella, Y. Hao, X. Li, Y. Wan, A. Rodríguez-Forteza, J. M. Poblet, L. Feng, N. Chen, *Inorg. Chem.* **2016**, 55, 1926–1933.
- [21] a) M. Murrie, *Chem. Soc. Rev.* **2010**, 39, 1986–1995; b) J. M. Frost, K. L. M. Harriman, M. Murugesu, *Chem. Sci.* **2016**, 7, 2470–2491.
- [22] F. Neese, *WIREs Comput. Mol. Sci.* **2012**, 2, 73–78.
- [23] a) D. Gatteschi, R. Sessoli, J. Villain, *Molecular Nanomagnets*, **2006**, Oxford University Press, Oxford; b) M. Atanasov, P. Comba, S. Helmle, D. Müller, F. Neese, *Inorg. Chem.* **2012**, 51, 12324–12335; c) S. K. Singh, G. Rajaraman, *Chem. Eur. J.* **2014**, 20, 5214–5218; d) S. Petit, G. Pilet, D. Luneau, L. Chibotaru, L. Ungur, *Dalton Trans.* **2007**, 4582–4588; e) R. Herchel, L. Vahovska, I. Potocnak, Z. Travnicek, *Inorg. Chem.* **2014**, 53, 5896–5898.
- [24] F. Weigend, R. Ahlrichs, *Phys. Chem. Chem. Phys.* **2005**, 7, 3297–3305.
- [25] a) F. Neese, *J. Am. Chem. Soc.* **2006**, 128, 10213–10222; b) F. Neese, E. I. Solomon, *Inorg. Chem.* **1998**, 37, 6568–6582; c) D. Maganas, S. Sottini, P. Kyritsis, E. J. J. Groenen, F. Neese, *Inorg. Chem.* **2011**, 50, 8741–8754; d) E. Cremades, E. Ruiz, *Inorg. Chem.* **2011**, 50, 4016–4020; e) S. Ye, F. Neese, *J. Chem. Theory Comput.* **2012**, 8, 2344–2351; f) R. Maurice, L. Vendier, J.-P. Costes, *Inorg. Chem.* **2011**, 50, 11075–11081.
- [26] a) C. Angeli, R. Cimraglia, S. Evangelisti, T. Leininger, J. P. Malrieu, *J. Chem. Phys.* **2001**, 114, 10252–10264; b) C. Angeli, R. Cimraglia, J. P. Malrieu, *Chem. Phys. Lett.* **2001**, 350, 297–305; c) C. Angeli, R. Cimraglia, J. P. Malrieu, *J. Chem. Phys.* **2002**, 117, 9138–9153; d) C. Angeli, S. Borini, M. Cestari, R. Cimraglia, *J. Chem. Phys.* **2004**, 121, 4043–4049.
- [27] a) S. S. Iyengar, H. B. Schlegel, G. A. Voth, *J. Phys. Chem. A* **2003**, 107, 7269–7277; b) S. S. Iyengar, *Theor. Chem. Acc.* **2006**, 116, 326–337.
- [28] A. D. Becke, *Phys. Rev. A: At., Mol. Opt. Phys.* **1988**, 38, 3098–3101.
- [29] P. C. Hariharan, J. A. Pople, *Theor. Chim. Acta* **1973**, 28, 213–222.
- [30] P. J. Hay, W. R. Wadt, *J. Chem. Phys.* **1985**, 82, 299–310.
- [31] H. B. Schlegel, S. S. Iyengar, X. Li, J. M. Millam, G. A. Voth, G. E. Scuseria, M. J. Frisch, *J. Chem. Phys.* **2002**, 117, 8694–8704.
- [32] Gaussian 09, M. J. Frisch, G. W. Trucks, H. B. Schlegel, G. E. Scuseria, M. A. Robb, J. R. Cheeseman, G. Scalmani, V. Barone, B. Mennucci, G. A. Petersson, H. Nakatsuji, M. Caricato, X. Li, H. P. Hratchian, A. F. Izmaylov, J. Bloino, G. Zheng, J. L. Sonnenberg, M. Hada, M. Ehara, K. Toyota, R. Fukuda, J. Hasegawa, M. Ishida, T. Nakajima, Y. Honda, O. Kitao, H. Nakai, T. Vreven, J. A. Montgomery, J. E. Peralta, F. Ogliaro, M. Bearpark, J. J. Heyd, E. Brothers, K. N. Kudin, V. N. Staroverov, R. Kobayashi, J. Normand, K. Raghavachari, A. Rendell, J. C. Burant, S. S. Iyengar, J. Tomasi, M. Cossi, N. Rega, J. M. Millam, M. Klene, J. E. Knox, J. B. Cross, V. Bakken, C. Adamo, J. Jaramillo, R. Gomperts, R. E. Stratmann, O. Yazyev, A. Austin, J. R. Cammi, C. Pomelli, J. W. Ochterski, R. L. Martin, K. Morokuma, V. G. Zakrzewski, G. A. Voth, P. Salvador, J. J. Dannenberg, S. Dapprich, A. D. Daniels, Ö. Farkas, J. B. Foresman, J. V. Ortiz, J. Cioslowski, D. J. Fox, **2009**.
- [33] a) A. Schäfer, H. Horn, R. Ahlrichs, *J. Chem. Phys.* **1992**, 97, 2571–2577; b) G. E. Scuseria, H. F. Schaefer III, *J. Chem. Phys.* **1989**, 90, 3700–3708.
- [34] a) A. A. Popov, S. Yang, L. Dunsch, *Chem. Rev.* **2013**, 113, 5989–6113; b) H. Kurihara, X. Lu, Y. Iiduka, N. Mizorogi, Z. Slanina, T. Tsuchiya, T. Akasaka, S. Nagase, *J. Am. Chem. Soc.* **2011**, 133, 2382–2385.
- [35] I. S. Bushmarinov, A. L. Konstantin, A. Mikhail Yu, *Russ. Chem. Rev.* **2009**, 78, 283–302.

Manuscript received: August 8, 2019

Revised manuscript received: September 5, 2019

Accepted manuscript online: September 11, 2019

Version of record online: December 12, 2019